APPLYING THE DMAIC METHOD FOR DEVELOPING A PVDF MATRIX COMPOSITE FOR INTEGRATED STRUCTURAL LOAD SENSING

A THESIS
SUBMITTED TO THE FACULTY OF
UNIVERSITY OF MINNESOTA
BY

Ghazaleh Haghiashtiani

IN PARTIAL FULFILLMENT OF THE REQUIREMENTS
FOR THE DEGREE OF MASTER OF SCIENCE

Adviser: Dr. Michael Greminger

August 2014

Acknowledgements

I would like to take this opportunity to appreciate the people who have helped and supported me throughout the completion of this work.

First, I would like to thank my adviser, Dr. Michael Greminger who taught me the basis of research, introduced me to this project, and guided me in every step of it.

I would like to appreciate my examining committee, Dr. Hongyi Chen and Mr. Moe Benda for the time they put in reviewing this thesis and their insightful recommendations.

I would like to thank Dr. Ping Zhao for letting me use the facilities in her lab for performing the required experiments; Dr. Emmanuel Enemuoh for showing me how to use the MTS machine; Mr. Jacob Dryke for showing me how to work with the compression molding equipment; Mr. Darrell Anderson and Mr. Mike Plante for machining my samples; and Mrs. Tracy Shaw for providing me the access to labs.

Finally, I would like to thank my parents and my siblings for their unconditional love and support, and all my friends who have supported me during the past two years.

Abstract

This thesis introduces a new carbon fiber reinforced composite structure that uses polyvinylidene difluoride (PVDF) as the matrix material instead of the polymers that are typically used. The piezoelectric properties of PVDF enable the proposed composite material to act both as the structure and as an integrated sensor for in situ structural health monitoring. In this study, the fabrication process, the polarization process, and the mechanical and piezoelectric characterization of the composite structure are discussed. In addition, the DMAIC method was applied to the polarization process in order to identify the factors affecting the degree of polarization. As part of the improve phase, a 2^3 factorial design of experiment (DOE) was performed to investigate the optimal conditions of the identified factors for the polarization process. Lastly, the future market potential of the proposed composite structure is explored by applying strategic market analysis tools including SWOT analysis, Ansoff's matrix, and technology S-curve.

Table of Contents

List of Tables

List of Figures

CHAPTER 1

INTRODUCTION

1.1 Thesis Overview

The necessity of continuous improvement has always been a robust part of every industry's strategic plan. The materials sector is not exempted from this norm. During the past years, many efforts have been made to develop and fabricate materials with advanced properties that can be used in a broad range of applications. For this purpose, either the properties of individual materials were enhanced, or multiple materials were combined together to create a composite material with superior properties. Among the materials used in developing composite structures, carbon fiber has attracted a lot of attention, and is being widely implemented in many different applications from aerospace structures to sporting equipment. This widespread use is mainly due to carbon fiber's high strength-to-weight ratio, but it also has the properties of high stiffness, electrical conductivity, and thermal conductivity (Chand, 2000).

In order to examine the safety and durability of structures, and to detect any damage or defect that can lead to catastrophic failures, structures need to be examined through a process called Structural Health Monitoring (SHM). For this purpose, different non-destructive evaluation (NDE) techniques can be adopted such as visual inspections,

ultrasonic methods, eddy currents, X-ray radiography, thermography, or shearography (Staszewski, Boller, & Tomlinson, 2004). However, all of these techniques have one of two limitations. They either do not allow the online monitoring of the structure during its operation, or they just allow the assessment of specific locations on the structure (Abot et al., 2010; Ong & Chiu, 2013). Moreover, in case of composite structures, the SHM process becomes even more complicated due to their different failure modes and the probability of inherent imperfections during the fabrication process (Kessler, Spearing, & Soutis, 2002; Lissenden & Rose, 2008).

A technology that has evolved in the recent years is the use of smart composite materials for the purpose of SHM. Smart materials have specific properties that enable them to react to external factors such as thermal, magnetic, electrical, or mechanical stimuli (Talbot, 2003). Consequently, these types of materials have a wide range of applications for sensing and actuating purposes. Embedding these smart materials in composite structures has resulted in self-sensing structures. In other words, these materials enable the structure itself to become the sensor and detect defects for SHM purposes. As suggested in literature (Akhras, 2000; Cao, Cudney, & Waser, 1999), this self-sensing capability of smart composite structures is analogous to the nervous system of the human body.

In this study, a new carbon fiber-reinforced polymer (CFRP) composite structure has been proposed. In this structure, the typical matrix material used in CFRPs has been replaced with the piezoelectric material polyvinylidene difluoride (PVDF). The

piezoelectric properties of PVDF will enable the proposed composite structure to have integrated sensing capabilities for structural health monitoring.

1.2 Related Works

Several efforts have been made to develop self-sensing composite structures. For instance, Abot et al. (2010) stitched a carbon nanotube (CNT) thread as a sensor into carbon/epoxy and glass/epoxy composite structures and used electrochemical impedance spectroscopy (EIS) to monitor the changes in the resistance of the sensor thread and as a result, detect strain and defects such as delamination (Abot et al., 2010). Loyola et al. (2013) spray-deposited a multi-walled carbon nanotube and PVDF (MWCNT-PVDF) thin film on a glass fiber mat and then used it in a glass fiber-reinforced polymer (GFRP). They implemented Electrical Impedance Tomography (EIT) to detect damage in the composite structure (Loyola et al., 2013). EIT is a method used for spatial imaging in which an array of electrodes is attached around the surface of the object being studied. Electric current is applied between a pair of the attached electrodes, while the resulting electric potential is recorded using the other remaining electrodes. This approach is repeated for all pairs of electrodes in order to achieve a complete profile for the object's conductivity or permittivity distribution (Saulnier, Blue, Newell, Isaacson, & Edic, 2001). Moreover, several works (Guemes & Menendez, 2002; Kuang, Kenny, Whelan, Cantwell, & Chalker, 2001; Leng & Asundi, 2003; Murukeshan, Chan, Ong, & Seah, 2000) have focused on embedding optical fiber Bragg grating (FBG) sensors within the composite structure to monitor the structure during the curing process and its operation. FBG refers to an optical fiber that has gratings inscribed on its core, which results in a

periodic change in the refractive index of the fiber's core. When a light passes through the FBG sensor, specific wavelengths will be reflected, while others will pass through the optical fiber.

The main difference between the smart composite structure proposed in this thesis and the previous works is that no external material is required to be inserted or woven into the composite structure. Thus, the fabrication process for the proposed material is the same as traditional thermoplastic matrix composites. In addition, the original properties of the reinforcement fabrics would not be affected.

1.3 Thesis Outline

This thesis is organized into seven chapters. The topics of each chapter are as follows:

In *Chapter 2*, the background information required for this project is provided. This chapter includes information regarding composite materials, polyvinylidene difluoride (PVDF), the piezoelectric effect, and the DMAIC method.

In *Chapter 3*, the research methodology used throughout the different phases of this project is discussed. This chapter addresses the techniques and methods used in sample preparation, sample polarization, and material characterization.

In *Chapter 4*, the details and the tools employed in each of the five phases of the DMAIC approach is discussed. In addition, this chapter presents the procedure and the results of the performed design of experiment (DOE).

In *Chapter 5*, the results of the proposed composite structure's characterization have been depicted, which includes the mechanical and piezoelectric characteristics of the composite and their comparison with values in other related works.

In *Chapter 6*, the proposed composite structure is treated as a product in development and is analyzed from the market perspective. This chapter focuses on assessing the future market potential of this composite.

Chapter 7 includes the discussion and concluding remarks. In addition, the future research directions are presented.

CHAPTER 2

BACKGROUND

2.1 Composite Materials

Composite materials, as suggested by the term itself, are made by combining two or more different materials in order to create a new material that has different properties than the individual properties of its constituents. The use of composite materials has its roots in ancient times where bricks were made from mud and straw (Jones, 1998). Today, composite materials are being widely used in a broad range of applications due to their superior properties.

As mentioned, composite materials are made of at least two different constituents. These constituents can be classified as the *matrix material* and the *reinforcement material*. Commonly, the reinforcement material determines the mechanical properties of the composite, including the strength and the stiffness. The reinforcement material can be either fibrous or particulate. Fiber reinforced composites can have continuous fibers (either unidirectional or multidirectional) or discontinuous fibers (with either random or preferred orientation). Particle reinforced composites can also have random or preferred dispersion. On the other hand, the matrix material binds the reinforcement materials together to create a structure. The most typical types of matrix materials are polymer,

ceramic, or metal (Matthews & Rawlings, 1999). Figure 1 illustrates some examples of composite structures (Matthews & Rawlings, 1999).

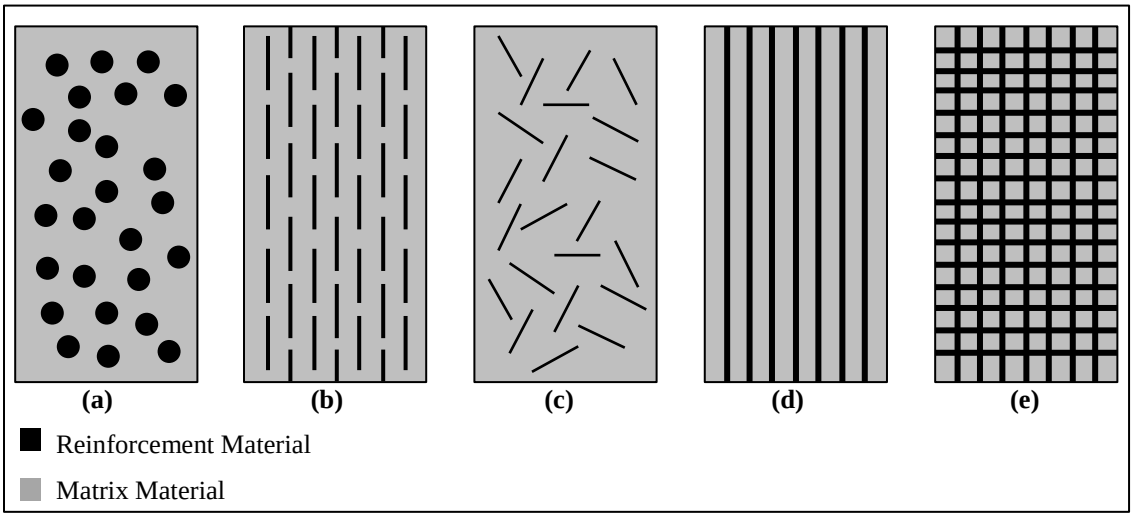

Figure 1. Examples of composite structures: (a) Particle reinforced with random dispersion; (b) discontinuous fibers with unidirectional orientation; (c) discontinuous fiber with random orientation; (d) unidirectional continuous fibers; and (e) bidirectional continuous fibers

Carbon Fiber reinforced composites are a type of composite structure where at least one of their reinforcement materials is carbon fiber. Carbon fiber's properties such as high strength, high stiffness, low weight, and electrical and thermal conductivity make it a desirable material for various applications (Chand, 2000). Moreover, the decreasing price of carbon fibers has broadened its applications (Chung, 1994). Some application areas for carbon fiber composites include aerospace structures, wind turbine blades, automobiles, military hardware, civil structures, and sporting equipment (Huang, 2009).

Like other composite structures, carbon fiber composites can have a polymer, metal, carbon, ceramic or a hybrid matrix. The polymer matrix composites are more easily manufactured due to their relatively lower processing temperature (Chung, 1994). Some examples of the polymers that are used in carbon fiber composites include

thermoset polymers, such as epoxy, phenolic, and furfuryl resin, or thermoplastic polymers, such as polyimide (PI), polyethersulfone (PES), polyetheretherketone (PEEK), polyetherimide (PEI), and polyphenyl sulfide (PPS) (Chung, 1994). Among the mentioned polymers, epoxy and PEEK are by far the most common polymers used in carbon fiber-reinforced composite structures. In this study, these commonly used polymer materials are replaced with the polymer polyvinylidene difluoride (PVDF) as the matrix material for developing a carbon fiber-reinforced composite. Polyvinylidene difluoride (PVDF) and its characteristics are discussed in detail in the following section.

2.2 Polyvinylidene difluoride (PVDF)

Polyvinylidene difluoride (PVDF) is a piezoelectric polymer material with the molecular formula of $(C_2H_2F_2)_n$ that is made by the polymerization of vinylidene difluoride. Today, PVDF is being fabricated in film, powder, or pellet forms (Dargaville et al., 2005). PVDF has a semi-crystalline structure, meaning that half of its molecules have an orderly and regular arrangement (Kepler & Anderson, 1992). Studies have identified four possible crystalline phases for PVDF, which are named alpha phase (α), beta phase (β), gamma phase (γ), and delta phase (δ). In each of these crystalline phases, PVDF material exhibits specific properties (Bloomfield, 1988). Moreover, these four phases can be transformed to each other by several different methods including electrical, thermal, and mechanical approaches (Bloomfield, 1988; Lovinger, 1982).

Among the four existing phases of PVDF, the alpha phase is the non-polar phase. In this phase, due to the symmetrical arrangement of molecules (see Figure 2(a)), the dipoles cancel out each other, resulting in a net dipole moment of zero (Sajkiewicz,

Wasiak, & Goclowski, 1999). The alpha phase has the lowest energy level of the four phases, and thus, is the most stable of the phases (Costa, Sencadas, Mano, & Lanceros-Méndez, 2006). The alpha phase is the dominant phase when the PVDF material is solidified after the melting process (Bloomfield, 1988; Lovinger, 1982). In contrast, the beta phase has high polarity due to the arrangement of molecules in its structure (see Figure 2(b)) and exhibits the highest ferroelectric response (Bloomfield, 1988; Costa et al., 2006). The dipoles of bulk PVDF in beta phase have random orientation. In order to be able to effectively exploit the piezoelectric properties, the dipole moments need to be rearranged to a specific orientation. This can be done by a polarization process in which a high electric field is applied to the PVDF material and, as a result, the dipoles are re-oriented along the direction of the applied electric field (see Figure 3) (Costa et al., 2006; Ramadan, Sameoto, & Evoy, 2014).

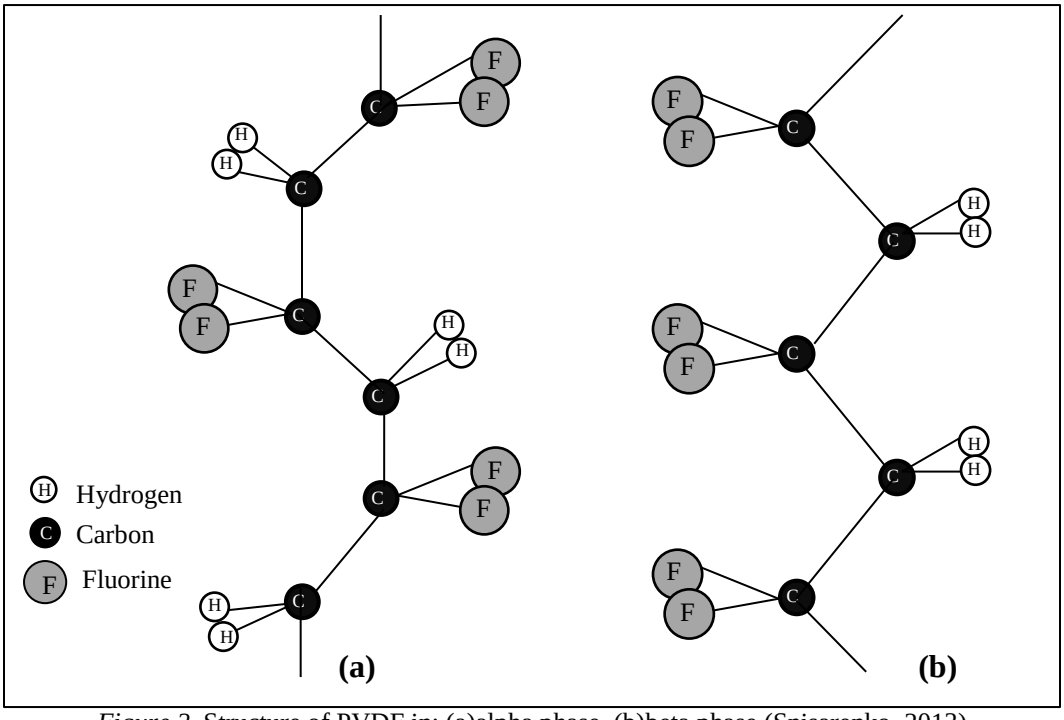

Figure 2. Structure of PVDF in: (a)alpha phase, (b)beta phase (Snisarenko, 2013)

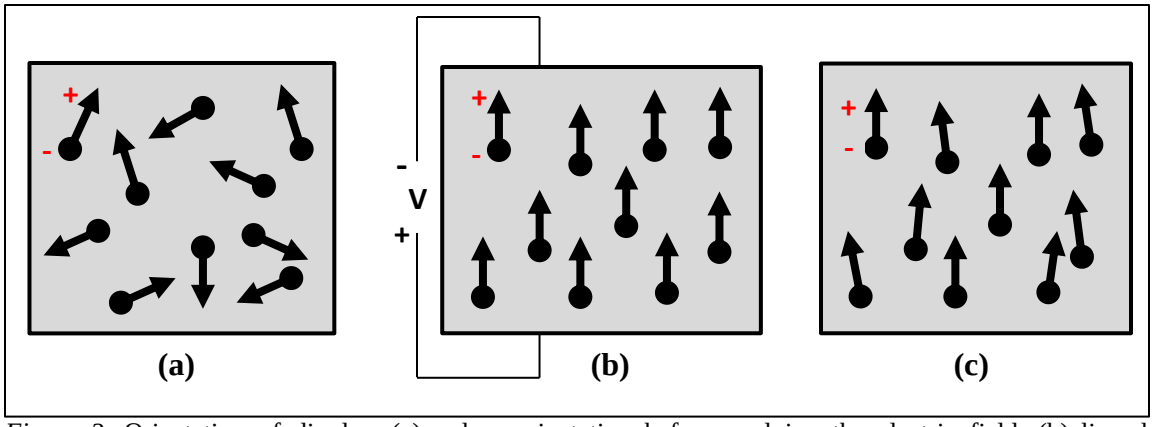

Figure 3. Orientation of dipoles; (a)random orientation before applying the electric field, (b)aligned orientation while applying the electric field, (c)remnant polarization after removing the electric field

Several methods have been discussed in the literature for transforming the non-polar alpha phase to the polar beta phase, which allows the material to be polarized to harness its piezoelectric properties. For instance, the application of high electric fields on the order of 1.25 MV/cm transforms the alpha phase to the delta phase. At this point, the delta phase can be transformed to the beta phase by applying an even higher electric field on the order of 5.3 MV/cm (Davis, McKinney, Broadhurst, & Roth, 1978; Lovinger, 1982). Alternatively, mechanical stretching of PVDF at elevated temperatures (below its melting point) can transform the material from the alpha phase to the beta phase. The effects of stretching rate and temperature on this phase transition have been studied in several works (Mohammadi, Yousefi, & Bellah, 2007; Sajkiewicz et al., 1999). Furthermore, the transition from alpha to beta phase can occur by annealing PVDF material under high pressure on the order of 4 *kbar* (Lovinger, 1982). Other methods discussed in the literature for making this transition include applying an electric field at high temperature (S. L. Hsu, Lu, Waldman, & Muthukumar, 1985), or quenching the PVDF material by cooling it down at very high rates (C. C. Hsu & Geil, 1984; Song,

Yang, & Feng, 1990). Finally, the beta phase can be achieved by creating artificial defects in PVDF structure by adding its copolymers such as trifluoroethylene (TrFE) or tetrafluoroethylene (TFE) (Dargaville et al., 2005).

As previously mentioned, PEEK is a common matrix material for carbon fiber-reinforced composite structures and in this study, we have replaced it with PVDF. Table 1 shows some of the properties of PEEK (Harper, 1999) and PVDF (Professional Plastics, n.d.).

Table 1
Comparison of the properties of PVDF with PEEK

Property	**Units**	**PVDF**	**PEEK**
Density	g/cm^3	1.77	1.32
Young's modulus	Gpa	1.724	3.5
Tensile Strength	Mpa	52.055	93.8
Melting Point	℃	165-170	334

From the above table, it can be understood that PEEK is stiffer and stronger than PVDF due to its higher modulus and tensile strength. On the other hand, PVDF has a lower melting temperature than PEEK, which leads to a fabrication process that is easier and consumes less energy.

In this study, the piezoelectric property of PVDF material is exploited in order to enable the proposed smart composite to have sensing capability. For this purpose, a polarization process should be performed to ensure the alignment of the dipole moments in the PVDF matrix of the composite structure so that the piezoelectric property can be harnessed. In the next section, the piezoelectric effect is discussed and its constitutive equations are presented.

2.3 Piezoelectricity

Piezoelectricity is a characteristic of crystalline materials. It was first discovered in quartz crystals (SiO_2) by the Curie brothers in 1880. The piezoelectric effect can be seen in natural crystals, some ceramics, and certain polymers (Fraden, 2010). When a mechanical stress is applied to a piezoelectric material, it will generate an electric charge proportional to the applied stress (direct piezoelectricity). In addition, if an electric voltage is applied to a piezoelectric material, the material experiences a mechanical strain proportional to the applied voltage (converse piezoelectricity) (Fraden, 2010; Ramadan et al., 2014). It should be noted that in order to collect the charge generated in the material due to the direct piezoelectric effect, conductive electrodes should be attached at two opposite sides of the material (Fraden, 2010). Piezoelectric materials have a broad range of applications in different industries including their usage in sensors, actuators, and other transducers (Tichý, Erhart, Kittinger, & Prívratská, 2010).

The matrix form of the simplified constitutive equations for the direct and converse piezoelectric effects are given respectively by the following equations (Moheimani & Fleming, 2006; Sirohi & Chopra, 2000):

$$\begin{bmatrix} D_1 \\ D_2 \\ D_3 \end{bmatrix} = \begin{bmatrix} 0 & 0 & 0 & 0 & d_{15} & 0 \\ 0 & 0 & 0 & d_{24} & 0 & 0 \\ d_{31} & d_{32} & d_{33} & 0 & 0 & 0 \end{bmatrix} \begin{bmatrix} \sigma_1 \\ \sigma_2 \\ \sigma_3 \\ \sigma_4 \\ \sigma_5 \\ \sigma_6 \end{bmatrix} + \begin{bmatrix} \varepsilon_{11}^{\sigma} & 0 & 0 \\ 0 & \varepsilon_{22}^{\sigma} & 0 \\ 0 & 0 & \varepsilon_{33}^{\sigma} \end{bmatrix} \begin{bmatrix} E_1 \\ E_2 \\ E_3 \end{bmatrix} \quad (1)$$

$$\begin{bmatrix} S_1 \\ S_2 \\ S_3 \\ S_4 \\ S_5 \\ S_6 \end{bmatrix} = \begin{bmatrix} s_{11}^E & s_{12}^E & s_{13}^E & 0 & 0 & 0 \\ s_{21}^E & s_{22}^E & s_{23}^E & 0 & 0 & 0 \\ s_{31}^E & s_{32}^E & s_{33}^E & 0 & 0 & 0 \\ 0 & 0 & 0 & s_{44}^E & 0 & 0 \\ 0 & 0 & 0 & 0 & s_{55}^E & 0 \\ 0 & 0 & 0 & 0 & 0 & s_{66}^E \end{bmatrix} \begin{bmatrix} \sigma_1 \\ \sigma_2 \\ \sigma_3 \\ \sigma_4 \\ \sigma_5 \\ \sigma_6 \end{bmatrix} + \begin{bmatrix} 0 & 0 & d_{31} \\ 0 & 0 & d_{32} \\ 0 & 0 & d_{33} \\ 0 & d_{24} & 0 \\ d_{15} & 0 & 0 \\ 0 & 0 & 0 \end{bmatrix} \begin{bmatrix} E_1 \\ E_2 \\ E_3 \end{bmatrix} \quad (2)$$

where:

S: Strain [*m/m*]

D: Electric displacement or electric charge displacement density [C/m^2]

σ: Stress [*N/m*], [*Pa*]

E: Electric field [*V/m*]

s^E: Elastic compliance constant at constant electric field [m^2/N]

d: Piezoelectric coefficient [*m/V*], [*C/N*]

ε^σ: Permittivity at constant stress [*F/m*]

For a sensor without an applied external electric field, the direct piezoelectric effect expressed by (1) can be re-written as follows (Sirohi & Chopra, 2000):

$$\begin{bmatrix} D_1 \\ D_2 \\ D_3 \end{bmatrix} = \begin{bmatrix} 0 & 0 & 0 & 0 & d_{15} & 0 \\ 0 & 0 & 0 & d_{24} & 0 & 0 \\ d_{31} & d_{32} & d_{33} & 0 & 0 & 0 \end{bmatrix} \begin{bmatrix} \sigma_1 \\ \sigma_2 \\ \sigma_3 \\ \sigma_4 \\ \sigma_5 \\ \sigma_6 \end{bmatrix} \quad (3)$$

For the direct piezoelectric effect, the piezoelectric coefficient's first subscript signifies the direction in which the generated charge is collected (perpendicular to the electrodes) and the second subscript shows the direction of applied stress on the material.

In this study, for the purpose of the piezoelectric characterization of the proposed smart composite material, the piezoelectric coefficients d_{31} and d_{33} will be investigated. Figure 4 illustrates a schematic of the settings for acquiring these two coefficients.

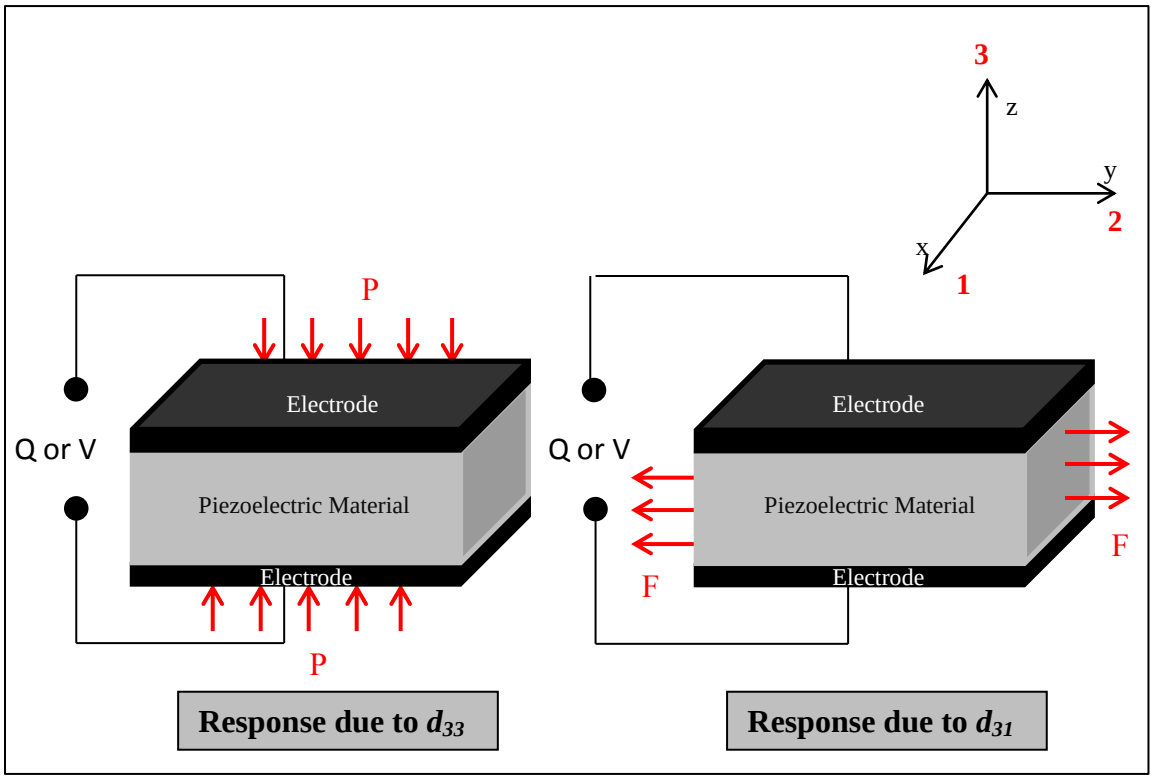

Figure 4. Schematic of the setting for characterizing the d_{33} and d_{31} coefficients

2.4 The DMAIC Method

Quality improvement through the use of quality management practices has always been a vital goal of businesses and organizations in order to remain competitive. Six sigma is a quality management strategy with the objectives of increasing customer satisfaction, enabling continuous improvement, reducing cost and waste, and eliminating defects (Thomas, Barton, & Chuke-Okafor, 2009; Tong, Tsung, & Yen, 2004). In the 1980s, Motorola initiated the implementation of six Sigma strategies and, subsequently, several different companies such as Allied Signal, Caterpillar, General Electric, Honeywell, IBM, Johnson Controls, and Sony have applied six sigma (Aboelmaged, 2010; Wang, 2008). Underlying the six sigma strategy is a framework abbreviated as

DMAIC, which stands for the five phases of define, measure, analyze, improve, and control. The five phases of DMAIC method are summarized below (Antony, 2014; George, 2002; Harmon, 2014; Li, Al-Refaie, & Cheng-Yu Yang, 2008; Sokovic, Pavletic, & Pipan, 2010; Tenera & Pinto, 2014; Tong et al., 2004).

Phase 1: Define. In this phase, the overview of the project being studied is presented and the process that requires improvement is identified. In addition, in the define phase, the Critical-to-Quality (CTQ) characteristic will be selected. CTQ refers to an output factor of the process identified for improvement, and acts as a criterion for evaluating the performance and enhancements of the process throughout the DMAIC method.

For the purpose of this study, a SIPOC diagram has been developed to map the different stages of the project by identifying the supplier, input, process, output, and customer. However, in a more formal setting, the implementation of a *Project Charter* has been suggested.

Phase 2: Measure. The main objective of the measure phase is to investigate the current performance of the process. Furthermore, the baseline factors that can affect the performance of the process are identified and initial data regarding the relation of these metrics with the CTQ will be collected.

Phase 3: Analyze. In this phase, all the potential input factors that can affect the output of the process and, as the result, the CTQ characteristic are identified. A cause-and-effect diagram (fishbone diagram) is a useful tool for this purpose, which is implemented in this study. Moreover, the identified parameters will be analyzed and the most critical ones are

chosen as the key process input variables (KPIV). The KPIVs are the input factors that have the highest impact on the CTQ characteristics.

Phase 4: Improve. In the improve phase, the process is optimized by finding the optimal condition of the KPIVs identified in the previous phase. The optimizations are then implemented to observe the improvements in the CTQ characteristic and the performance of the process. One of the useful tools in this phase is Design of Experiment (DOE). DOE is a technique that can be used to investigate the impact of different independent factors on the response of a process, the interaction between those factors, and their optimum condition for generating the best output (Mathews, 2005). A special case of DOE that has been used in this study is a 2^k full factorial DOE, in which the effects of k factors are investigated at two levels (typically a low and a high level) of their value. Since only two levels of each factor are being studied, any nonlinearity between the input and output parameters will not be captured (Montgomery, 2008).

Phase 5: Control. In the last step of the DMAIC method, the focus is on developing efficient strategies to sustain the resulted improvements. This includes identifying the future potential failures that can occur in the process, and developing efficient strategies to detect and prevent them. In this study, a failure mode and effects analysis (FMEA) is performed to address this concern.

CHAPTER 3

RESEARCH METHODOLOGY

3.1 Sample Preparation

The proposed composite structure is made of two layers of carbon fiber as the main reinforcement material. As mentioned earlier, carbon fibers are electrically conductive. Consequently, they also act as the electrodes for the purpose of sensing. Moreover, in order to prevent the two layers of carbon fiber material from shorting to each other, one layer of Kevlar fabric has been placed between them to act as a dielectric layer. Kevlar is a para-aramid fiber developed by DuPont Company. The tensile modulus and strength of Kevlar are close to those of carbon fiber (Deteresa, Allen, Farris, & Porter, 1984; Kollár & Springer, 2003). As a result, using this material has a minor effect on the overall strength and mechanical properties of the composite structure. These three layers of reinforcement materials are bonded to each other using PVDF films as the matrix material. Two layers of PVDF film are placed between each pair of reinforcement fabrics and on the top and bottom of the composite structure. Figure 5 depicts the structure of the samples.

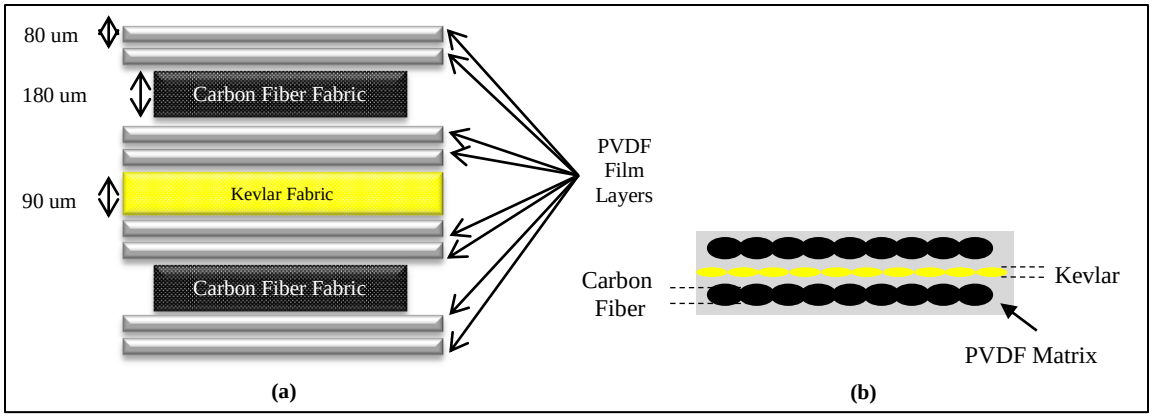

Figure 5. Schematic of the composite structure and material thicknesses; the stack-up of reinforcement fabrics and PVDF film layers (a) before melting, (b) after melting

The final samples are prepared by heating the stack-up of materials under a pressure of 7.164 *kpa* at 200℃ for a duration of 4 hours. This setting assures the complete melting of PVDF films and bonding of the composite layers. Figure 6 illustrates the microscopic view of the final sample's cross section. The proposed structure acts as a capacitor due to electric conductivity of carbon fiber and dielectric effect of Kevlar. The capacitance of the 100 $mm \times 80$ mm samples was measured to be between 800 and 900 pF.

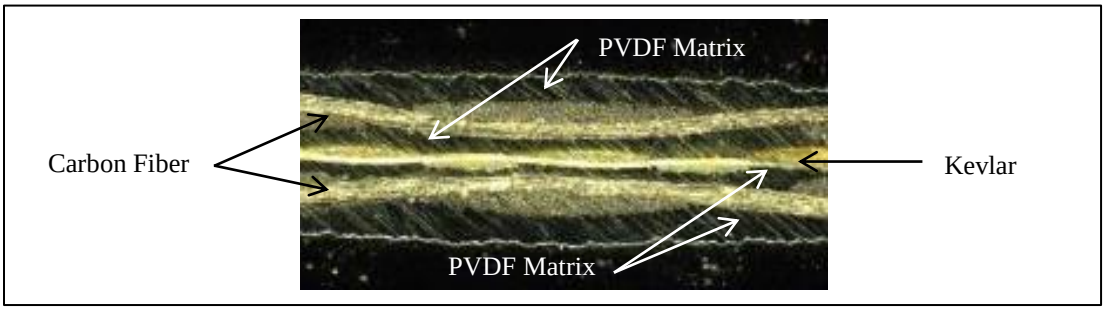

Figure 6. Microscopic view of sample's cross section

For the purpose of this study, these samples will be used in a tensile test. If the samples were place in the tensile test machine using the structure shown in Figure 5(a), the grips of the machine would cause a compression on the sample, which would affect

the tensile test's results. In order to prevent this error, the composite structure shown in Figure 5(a) was further extended by adding two layers of Kevlar on each side of the sample along with two layers of PVDF on top and bottom (see Figure 7 and 8(c)). Using this extended structure, the attached layers of Kevlar are placed between the grips and, as a result, no pressure is applied to the carbon fiber electrodes during the tensile test.

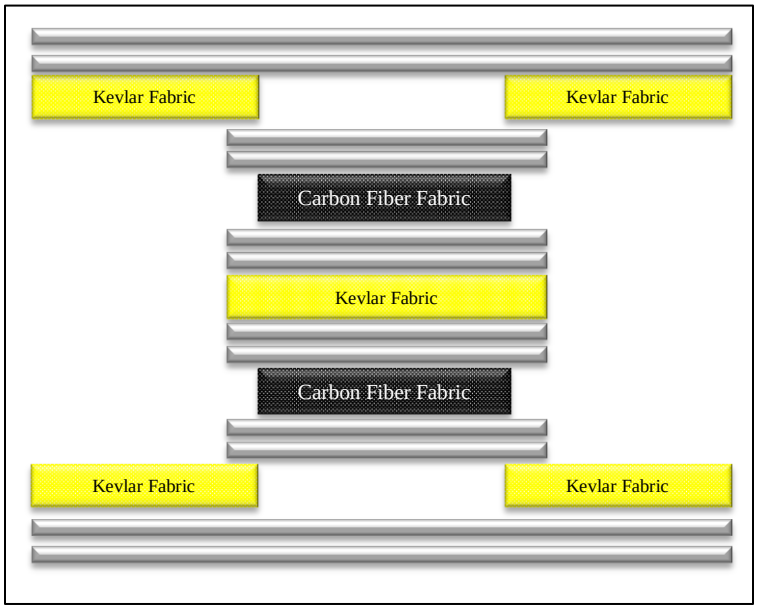

Figure 7. Extended structure for composite samples

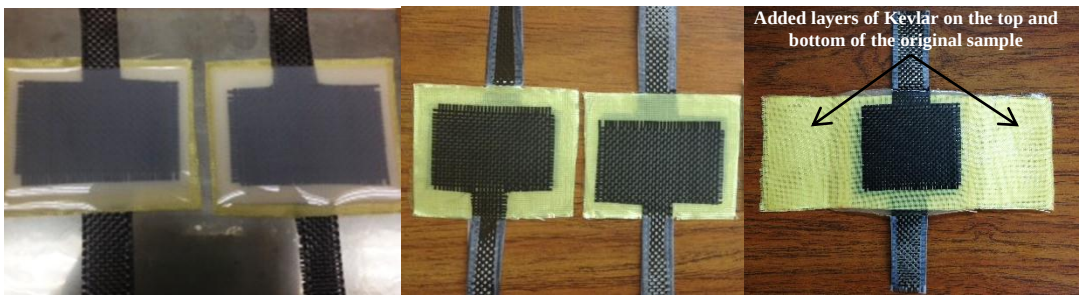

Figure 8. Prepared samples (a) original samples before melting the PVDF films, (b) original samples after melting the PVDF films, (c) extended sample for tensile testing.

3.2 Sample Polarization

3.2.1 Initial Polarization Process

The PVDF material needs to be polarized to align the dipole moments of its crystalline structure so that it can generate a piezoelectric response due to an applied load. As mentioned earlier, after PVDF films are melted and cooled down, the dominant phase of their crystalline structure is the alpha phase, which is non-polar. Several different methods were discussed in Section 2.2 for transforming the alpha phase to the polar beta phase to allow polarizing the PVDF material. However, due to the nature of the composite structure in this study, the previously discussed methods are not applicable. For instance, the mechanical stretching of the composite structure is not possible for this case because the reinforcement layers of carbon fiber and Kevlar prevent large strains from being applied. Moreover, the application of large electric fields in the order of 5.3 MV/cm for polarization is also not possible for the composite structure proposed in this study due to the inevitable dielectric breakdown caused by irregularities in the carbon fiber-Kevlar structure, which results in the short-circuiting of the samples.

Due to the above mentioned limitations, finding an effective approach for polarizing the PVDF matrix was the most challenging part in preparing the proposed smart composite material. The initial process that was adopted for polarization included the use of a high voltage source and a modified Sawyer-Tower circuit (Etzold, 2000) for applying a cyclical electric field, while placing the samples on a hot plate for adding the factor of temperature to the polarization process. The modified Sawyer-Tower circuit (see Figure 9) included Zener diodes to protect the Analog-to-Digital Converter (ADC)

equipment from sample shorting. In this method, a triangle wave with an amplitude of 2000 volts at the frequency of 0.2 *Hz* was applied as the voltage excitation at several different temperatures. Using LabVIEW software, the output of this test was obtained as a hysteresis plot (polarization-electric field or P-E loop) at each tested temperature. This plot represents the polarization or the charge developed in the samples due to the applied electrical field at a specific frequency (Stewart, Cain, & Hall, 1999).

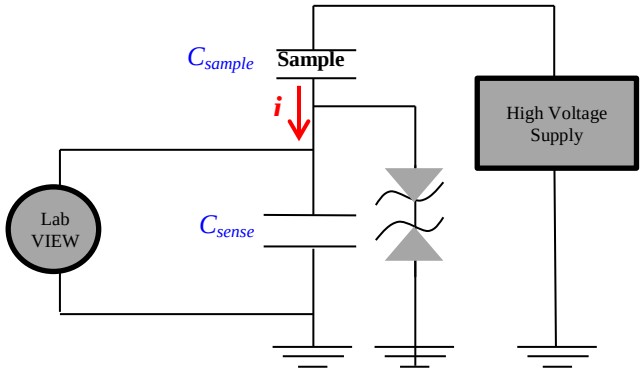

Figure 9. Schematic of the circuit used for initial polarization and for generating hysteresis plots (P-E loops).

The charge developed on the sense capacitor in Figure 9 can be expressed by:

$$Q(t) = C_{sense}V = \int_0^t idt \tag{4}$$

Where i is the current generated by the response of the samples due to the cyclical applied voltage and it can be formulated as follows (Dickens, Balizer, DeReggi, & Roth, 1992):

$$i = \frac{C_{sample}dV}{dt} + \frac{AdP}{dt} + \frac{V}{R_{sample}} \tag{5}$$

In (5), C is the sample's capacitance, A is the area, P is the polarization, t is time, V is the applied voltage, and R is the sample's resistance. In other words, the three terms in (5) represent the response of the sample due to its capacitance, ferroelectricity, and resistance respectively.

In order to generate the hysteresis loop, the second term of (5) is desired. Consequently, to determine the polarization, the capacitive and resistive responses should be compensated for. However, the capacitive response is in phase with the polarization and it does not affect the measurement of the remnant polarization. On the other hand, the resistive response is not in the same phase with polarization and has a 90 degrees phase lag. Consequently, in order to compensate for this, the resistance of the samples was measured and the resistance compensation was performed in the LabVIEW program by subtracting the integration of the third term from the sample's response.

3.2.2 Improved Polarization Process

Later in this study, the polarization process was improved by adding the factor of time. In this new process, using a DC voltage source a constant voltage was applied to the sample for a specific period while the sample was placed on a hot plate at a specified temperature. Figure 10 shows the setting of this process.

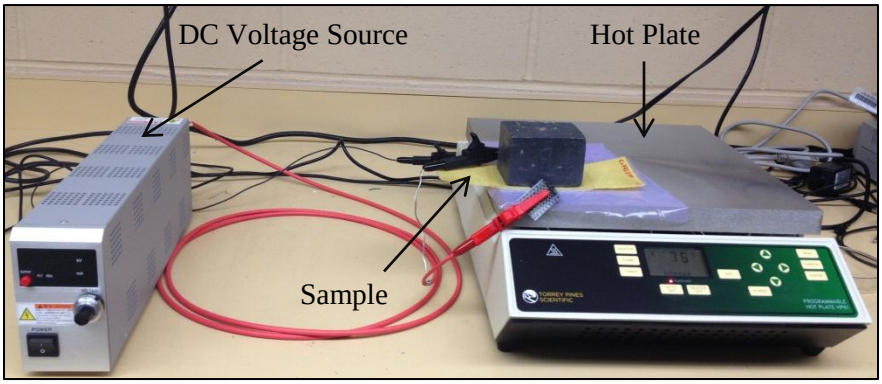

Figure 10. Setting of the new polarization process

This process was optimized by applying the DMAIC method and performing a DOE (Design of Experiment) in order to find the optimal condition of voltage,

temperature, and duration of poling to increase the sample's response and degree of polarization.

3.3 Sample Characterization

3.3.1 Mechanical Characterization

For the mechanical characterization, the Young's modulus (*E*) was investigated as a measure for stiffness of the proposed composite structure. For this purpose, a tensile test was performed on the samples using MTS (Material Testing System) equipment. The composite sample was placed between the grips of the testing equipment and an extensometer was attached to it in order to monitor the strain developed in the sample due to an applied tensile load. Figure 11 shows the setting of this experiment.

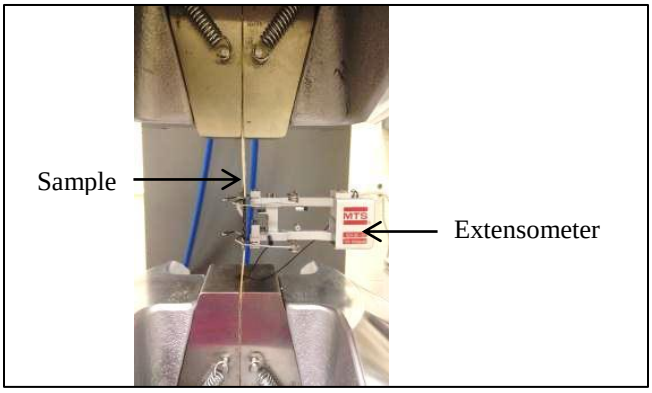

Figure 11. Test setting for finding the Young's modulus

This test results in the stress-strain plot for the composite structure. The slope of the stress-strain plot is the Young's modulus.

This experiment was also performed on separate samples using only carbon fiber and Kevlar reinforcements in order to find the relative Young's modulus for each of these materials, which was used in the calculations that are discussed in detail in Chapter 5. See Figure 12 for the composition of these samples.

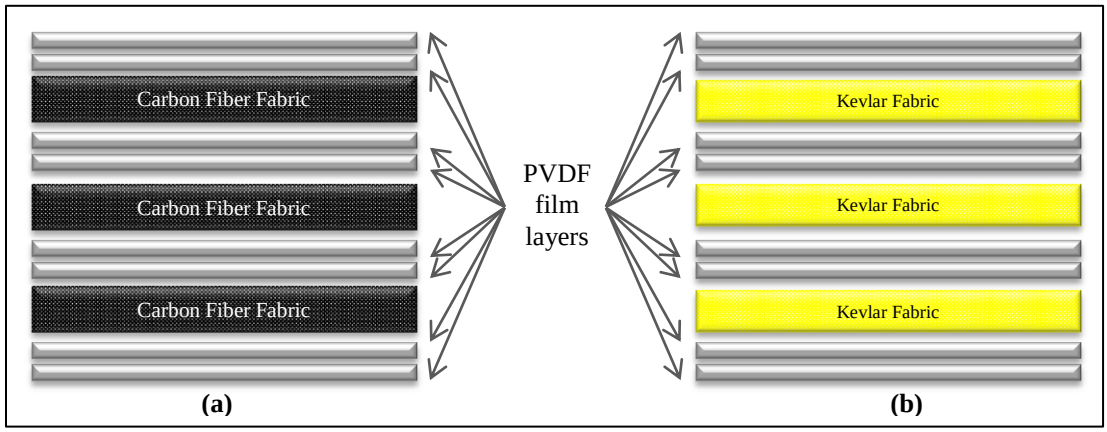

Figure 12. Sample structure used for finding the Young's modulus for individual reinforcement materials: (a) carbon fiber, (b) Kevlar

3.3.2 Piezoelectric Characterization

In order to characterize the piezoelectric properties of the composite structure, the d_{31} and d_{33} coefficients were investigated. Prior to performing the required experiments for finding these coefficients, the frequency influence on the sample's response was studied in order to find an optimal frequency for performing the tests. For this purpose, the sample's response was quantified as the ratio of the charge developed in the sample to the applied force at 10 different frequencies from 0.01 *Hz* to 20 *Hz* in a tensile test. The experiment was performed for two different samples. The results are shown in Figure 13.

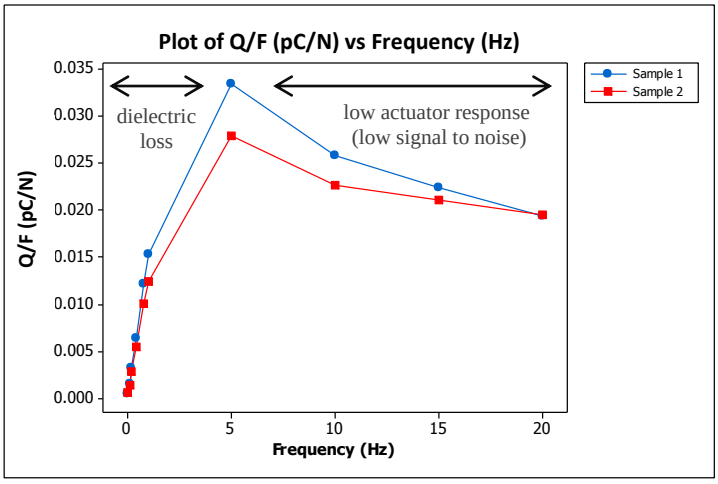

Figure 13. Composite sample's response at different frequencies in tensile test

As it can be seen in Figure 13, at lower frequencies, the response of the samples is low due to dielectric loss. At higher frequencies, there is low actuator response due to the mechanical limitations of the tensile testing machine. In other words, the equipment's noise dominates the actual signal in higher frequencies. From the frequencies that were tested, 5 *Hz* was chosen for performing the tensile and compression tests in order to measure the d_{31} and d_{33} coefficients, respectively.

For calculating the d_{31} coefficient, a tensile test was performed on the composite samples. The setting used for the tensile test is shown in Figure 14(a). A cyclic force with the amplitude of about 15 *N* was applied to the sample at the frequency of 5 *Hz*. The charge generated in the sample due to the applied tension was extracted as the output. In order to find the effective d_{31} coefficient, the force that is applied to the middle layer of the composite structure (between the two carbon fiber electrode layers) needs to be known. For this purpose, the two carbon fiber layers and the layer between them (consisting of Kevlar and PVDF matrix) are assumed to be three parallel springs (see Figure 14(b)). Knowing that parallel springs have equal displacements, the following equations can be written:

$$\delta_{CF} = \delta_{K+PVDF} \rightarrow \frac{F_{CF}L_{CF}}{E_{CF}A_{CF}} = \frac{F_{K+PVDF}L_{K+PVDF}}{E_{K+PVDF}A_{K+PVDF}} \quad (6)$$

$$F_{tot} = 2F_{CF} + F_{K+PVDF} \quad (7)$$

Where $\delta, F, L, E,$ and A are respectively the displacement, force, length, Young's modulus, and area of each layer as indicated by the given subscript (*CF*: Carbon Fiber; *K*: Kevlar; *K+PVDF*: the middle layer between two carbon fiber electrodes). Equation (6) and (7) can be solved for F_{CF}(force applied on each carbon fiber layer) and F_{K+PVDF}

(force applied on the middle layer consisting of Kevlar and PVDF matrix). Knowing the force applied to the middle layer, the stress (σ_{K+PVDF}) can be determined ($\sigma_{K+PVDF} = \frac{F_{K+PVDF}}{A_{K+PVDF}}$, where $A_{K+PVDF}$is the cross-sectional area of the middle layer). Finally, the effective d_{31} can be calculated as follows:

$$(d_{31})_{eff} = \frac{Q/A_{CF,electrode}}{\sigma_{K+PVDF}} \quad (8)$$

Where Q is the charge developed in the samples during the tensile test, A is the area of the carbon fiber electrodes, and σ_{K+PVDF} is the stress applied to the middle layer of the sample.

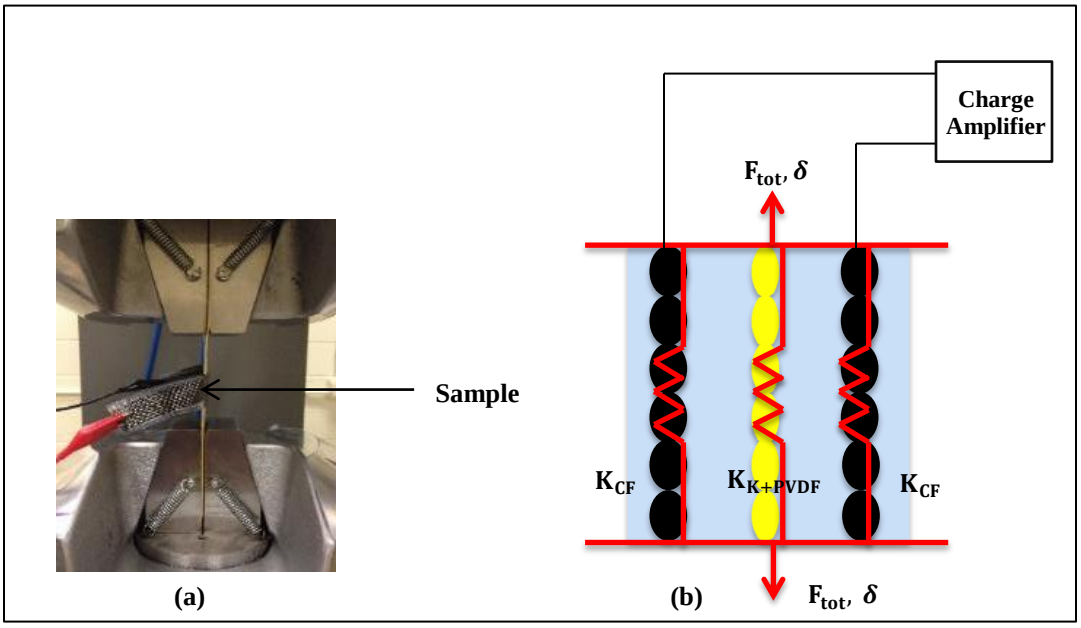

Figure 14. Test setting for finding the d_{31} coefficient, (a)experimental setting, (b) schematic of the assumed parallel springs

In order to find the d_{33} coefficient, compression test was performed on the samples. The setting used for the compression test is shown in Figure 15(a). A cyclic compression force with the amplitude of 179.36 N was applied to the sample at the

frequency of 5 *Hz*. The charge generated in the sample due to the applied compression was extracted as the output.

As it can be seen in Figure 15(b), in the compression case the stress applied to the effective layer (the middle layer consisting of Kevlar and PVDF) is equal to the total stress. Consequently, the experimental value of $(d_{33})_{eff}$ can be calculated as follows:

$$(d_{33})_{eff} = \frac{Q/A_{CF,electrode}}{\sigma_{K+PVDF}} \quad (9)$$

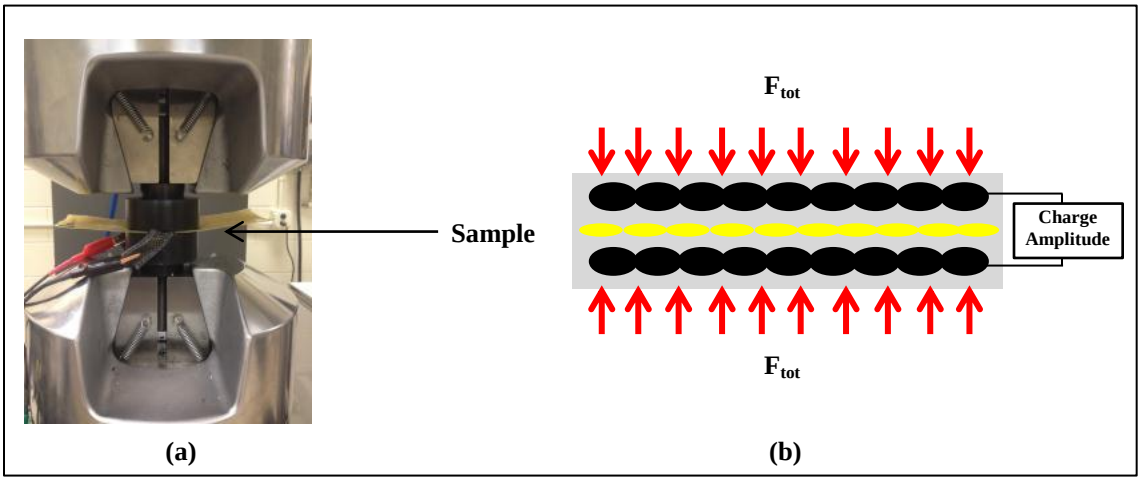

Figure 15. Test setting for finding the d_{33} coefficient, (a) Experimental setting, (b)Schematic of the applied load

The experimental value of $(d_{33})_{eff}$ was then substituted in the following equation, which represents the formulation for effective d_{33} coefficient for a piezoelectric composite with layer arrangement as the composite structure proposed in this study (Neelakanta, 1995).

$$(d_{33})_{eff} = \frac{\upsilon_{PVDF}(d_{33})_{PVDF}(\varepsilon_{33})_{Kevlar} + \upsilon_{Kevlar}(d_{33})_{Kevlar}(\varepsilon_{33})_{PVDF}}{\upsilon_{PVDF}(\varepsilon_{33})_{Kevlar} + \upsilon_{Kevlar}(\varepsilon_{33})_{PVDF}} \quad (10)$$

Where v_{PVDF} and v_{Kevlar} signify the volume fraction of PVDF and Kevlar in the effective layer, and $(\varepsilon_{33})_{PVDF}$ and $(\varepsilon_{33})_{Kevlar}$ represent the permittivity constant of PVDF and Kevlar, respectively.

Equation (10) was back solved for $(d_{33})_{PVDF}$. The results were compared to the literature values for $(d_{33})_{PVDF}$ in order to investigate the degree of polarization of the samples.

CHAPTER 4

APPLYING THE DMAIC METHOD TO IMPROVE THE POLARIZATION PROCESS

4.1 Define Phase

In order to define the manufacturing process for the proposed smart composite, an SIPOC diagram has been developed as shown in Figure 16.

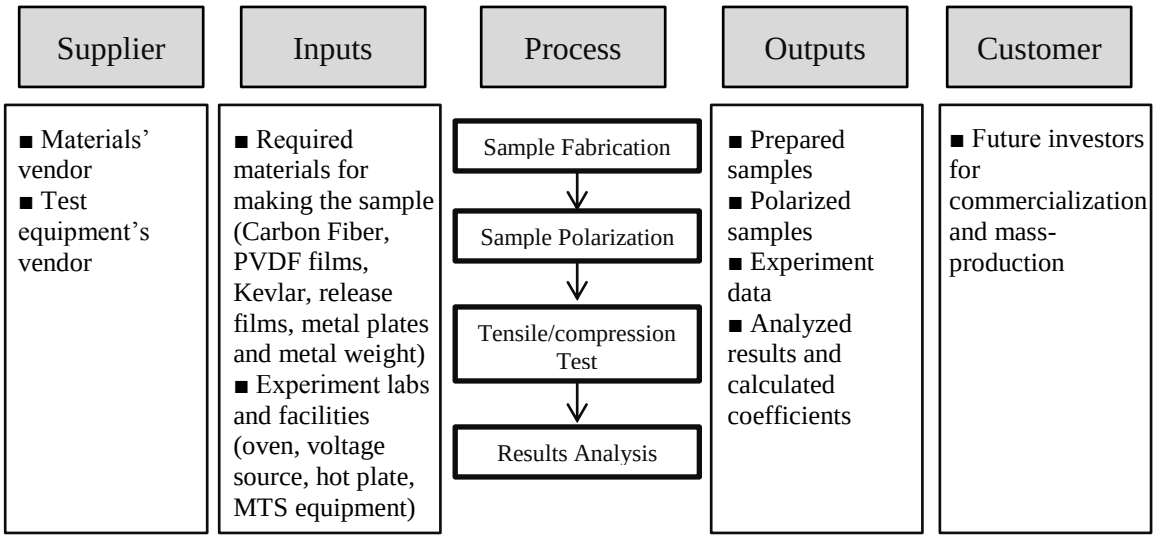

Figure 16. SIPOC diagram

As it can be seen in the SIPOC diagram, this study includes four main steps; first, the samples of the proposed composite structure are fabricated. Second, the prepared samples were polarized so that their piezoelectric properties can be exploited. Then, the samples are exposed to applied loads in order to examine their response and load sensing

potential. Finally, the results obtained in the last step are analyzed in order to calculate the ratio of the charge developed in the sample to the applied force (Charge/Force or *Q/F*), which helps in evaluating the structure's response and the effectiveness of the polarization. Therefore, the ratio of the charge developed in the sample to the applied force is determined as the critical-to-quality characteristic (CTQ). The problem in this experiment lies in the polarization phase where the factors affecting the polarization and their optimal values need to be investigated. Consequently, the purpose of applying the DMAIC method in this study is to improve the polarization process and as a result, the CTQ characteristic.

4.2 Measure Phase

The initial process that was employed for polarization was discussed in detail in Section 3.2.1. In this process, a cyclical electric field was applied to the sample using a triangular wave at a specific temperature and the hysteresis loop was obtained. Figure 17 shows the results of this process by applying 2000 volts at six different temperatures (T= 25℃,50℃,75℃, 100℃, 125℃, and 150 ℃). For obtaining the hysteresis plots, a frequency of 0.2 *Hz* is used that results in a polarization period of 2.5 seconds for the positive portion of the triangle signal.

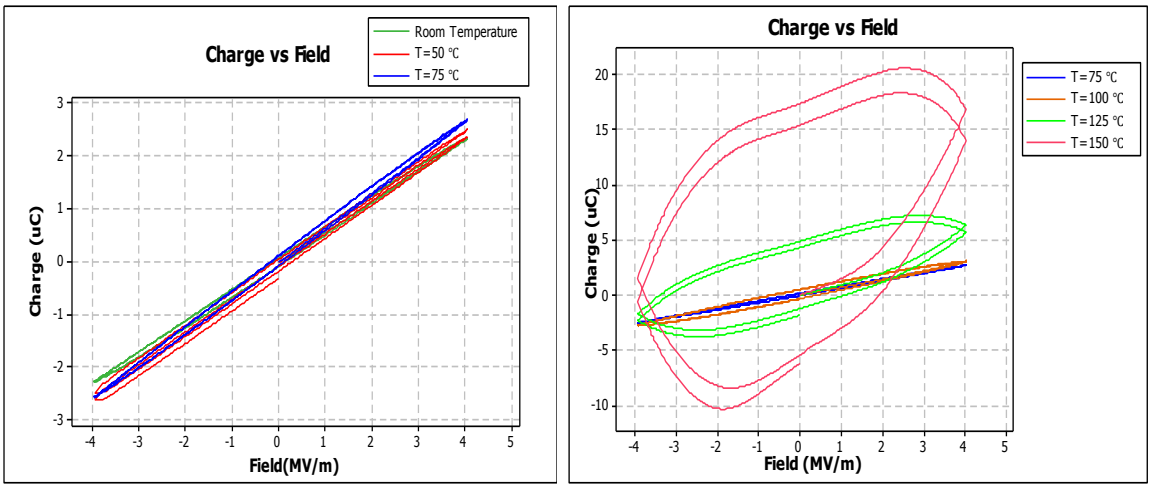

Figure 17. Hysteresis plots obtained at *V*=2000 *volts* and different temperatures

The *x*-intercept of hysteresis plot signifies the coercive field (E_c), which is the electric field required to make the polarization zero. The *y*-intercept of the hysteresis plot shows the remnant polarization (P_r), which is the amount of polarization that remains in the sample when the applied electric field becomes zero (Bhalla et al., 1986). The results of the initial polarization process suggested that temperature definitely has an impact on the polarization of the samples. However, since in higher temperatures leakage current occurs as suggested by the shape of the hysteresis plots, it cannot certainly be said that higher temperature are better for polarization process. Therefore, the effect of this factor should be further investigated along with the other factors that will be determined in the next phase.

4.3 Analyze Phase

In this phase, the input factors that can affect the CTQ characteristic will be determined and the KPIVs are selected. For this purpose a cause-and-effect diagram, also known as the Fishbone diagram, is used. The results are shown in Figure 18.

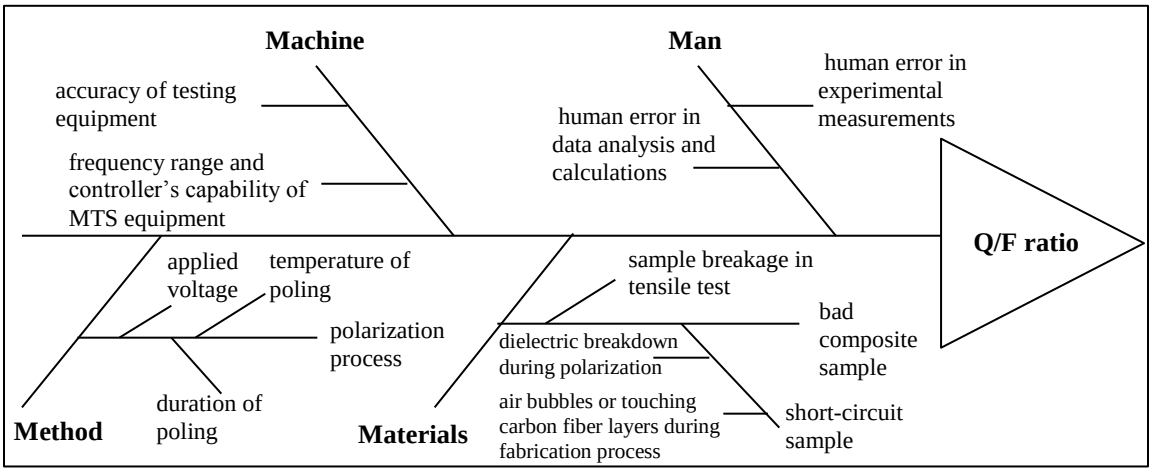

Figure 18. Cause-and-Effect diagram

Going through the cause-and-effect diagram, the polarization process and its contributing factors (temperature, voltage, and duration of poling) seem to have the most direct impact on the response of the samples in tensile test and the *Q/F* ratio. This is due to the fact the other factors shown on the fishbone diagram have a known relationship to the CTQ, however, the optimal condition of these three factors for generating the highest response is unknown. Consequently, the three factors of voltage, temperature and duration of poling are selected as the KPIVs. In order to find the optimal condition of these factors, the design of experiment method was applied in the improve phase.

4.4 Improve Phase

In order to find the optimal conditions of the factors identified in the previous phase, and their effect on sample's polarization, a 2^3 full factorial DOE was performed. The settings of the conducted experiments and their results are discussed in the following sections.

4.4.1 DOE Setting and Procedure

The input factors that were studied in the DOE were voltage, temperature, and duration of poling. The experiments were conducted at two levels of each factor. Table 2 shows these factors and their values at each level.

Table 2
Design of Experiment input factors and their settings

Factor	**Low Level**	**High Level**
Temperature	50 ℃	150 ℃
Voltage	1000 *V*	2000 *V*
Duration of Poling	5 *min.*	20 *min.*

In each of the runs, a constant voltage was applied to the sample for a specific period while the sample was placed on a hot plate at the specified temperature. After the polarization step, the response of the samples was monitored in the tensile test and the ratio of the charge developed in the sample to the applied force was calculated as the experiment's output (Q/F). For the reliability of the results, each of the experiments was replicated two times resulting in 16 runs. Table 3 shows the settings of each of the runs.

The results obtained from the DoE were analyzed using Minitab 16 software as discussed in the following sections.

Table 3
Input factors' setting in each of DoE runs and the obtained output

	Input Factors			Output
Run	**Voltage**	**Temperature**	**Duration of Poling**	**Q/F (pC/N)**
1	High	High	High	0.0063
2	High	High	High	0.0077
3	High	High	Low	0.0066
4	High	High	Low	0.0052
5	High	Low	High	0.0192
6	High	Low	High	0.0848
7	High	Low	Low	0.0076
8	High	Low	Low	0.0088
9	Low	High	High	0.0028
10	Low	High	High	0.0038
11	Low	High	Low	0.0017
12	Low	High	Low	0.0015
13	Low	Low	High	0.0090
14	Low	Low	High	0.0109
15	Low	Low	Low	0.0048
16	Low	Low	Low	0.0056

4.4.3 Main Effect Plots

The main effect plots depict the effect of the change in each of the factors on the response. The main effect plots for temperature, voltage, and duration of poling are shown in Figure 19.

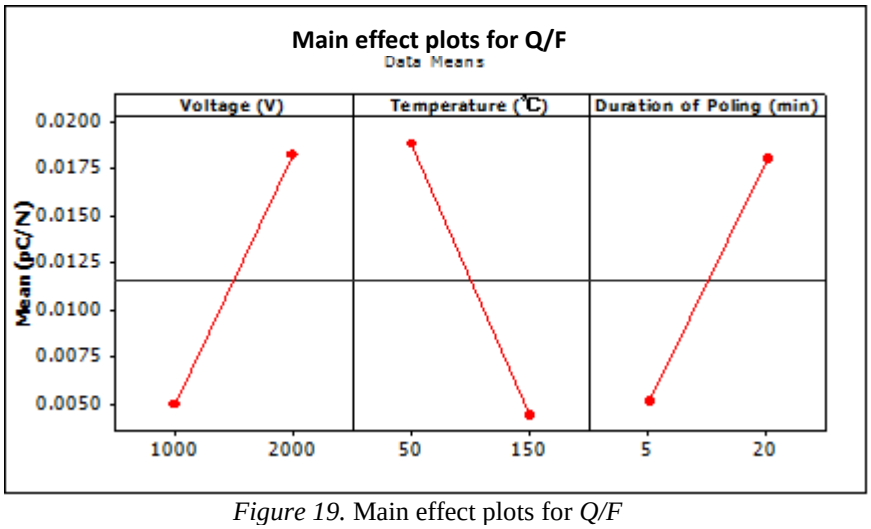

Figure 19. Main effect plots for *Q/F*

As it can be seen in Figure 19, changing the voltage and duration of poling from their low level to their high level will cause an increase on the response of the sample. On the other hand, changing the temperature from its low level to its high level will decrease the response.

4.4.4 Interaction Plot

Figure 20 illustrates the interactions between each pair of the factors. In addition, for each pair, it shows the sensitivity of the response to the changes of one factor at a specified level of the other.

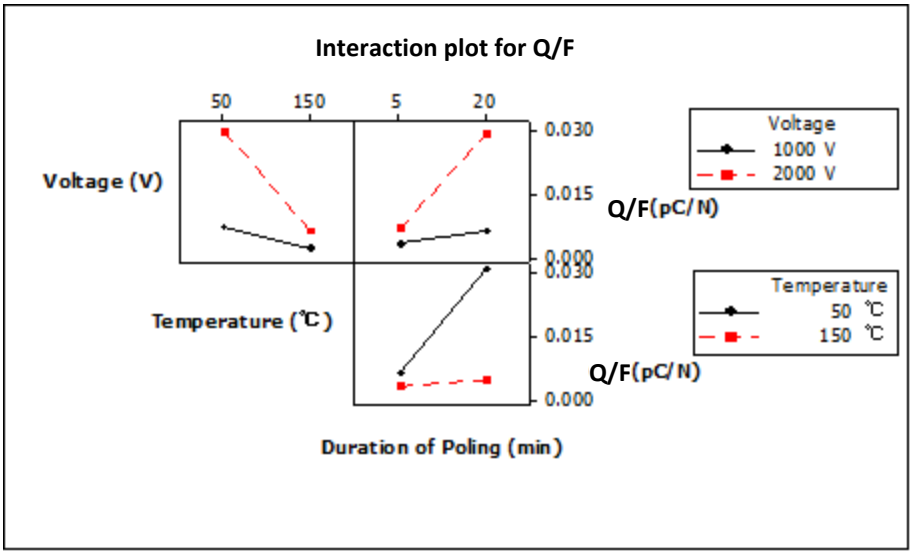

Figure 20. Interaction plot for *Q/F*

The fact that each pair of lines has different slopes signifies that all the factors have significant interactions. According to the voltage and temperature interaction plot, the response has a higher value at 50℃ than 150℃ for both levels of voltage. Also, the response is more sensitive to the changes of temperature at the high level of voltage. The voltage and duration of poling interaction plot suggests that the response for poling at the

duration of 20 minutes is higher than 5 minutes for both levels of voltage and it is more sensitive to the changes of duration of poling at the high level of voltage. Finally, the temperature and duration of poling interaction plot shows that poling the samples for a longer duration (20 minutes) causes a higher response than shorter duration (5 minutes) for both levels of temperature. In addition, the response is more sensitive to the changes in the duration of poling at the low level of temperature.

4.4.5 Finding the Optimal Temperature

According to the above results, samples generate higher response when they have been polarized at the higher levels of voltage and duration of poling, and at the lower level of temperature. However, since temperature had a negative impact on the response and based on the fact that the performed two-level DOE would not capture the potential nonlinearities, the lower level of temperature (T=50℃) could not be accepted as the optimal condition. Therefore, it was postulated that the samples have a higher response at a temperature between 50℃ and 150℃. In order to find that optimal temperature, a single factor experiment was performed for different temperatures between 50℃ and 150℃ (T=75℃, 100℃, and 125℃) at the high levels of voltage and duration of poling. For the integrity of the experiment, each of the runs was replicated two times, resulting in 10 runs. Table 4 shows the settings of the input factors and the value of the output for each of the runs.

Table 4
Optimal temperature experiment input factors setting and output values

	Input			Output
Run	**Voltage**	**Duration of Poling**	**Temperature**	**Q/F (pC/N)**
1	High	High	50	0.0090
2	High	High	50	0.0081
3	High	High	75	0.0205
4	High	High	75	0.0182
5	High	High	100	0.0118
6	High	High	100	0.0098
7	High	High	125	0.0159
8	High	High	125	0.0130
9	High	High	150	0.0063
10	High	High	150	0.0077

The results as shown in Figure 21 suggest that the relationship between the *Q/F* ratio and temperature is non-linear, which could not be captured with a two level DOE. The results indicate that for the tested temperatures, the samples generate the highest response at 75 ℃ .

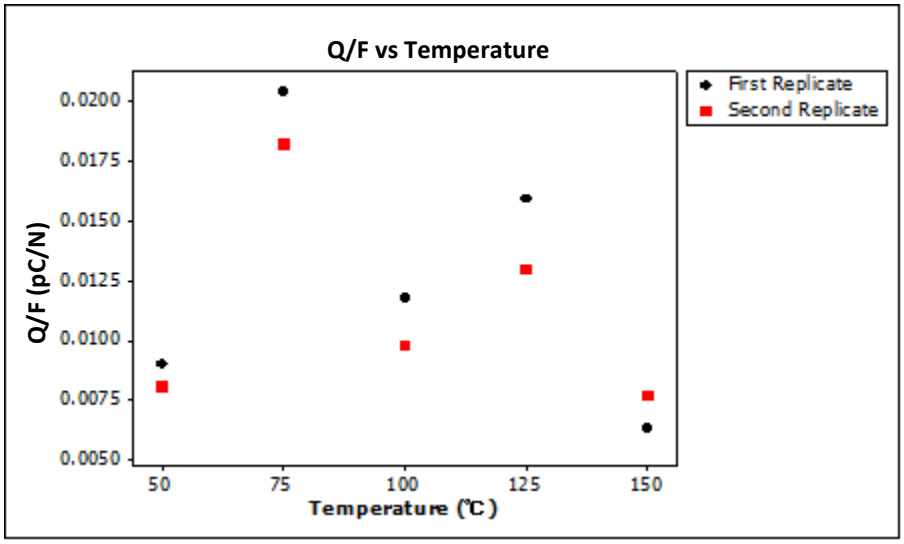

Figure 21. Sample's response at different temperatures

For this study, the optimal condition of the polarization factors were found to be *V*=2000 volts, *T*= 75℃, and duration of poling= 20 minutes. A point that is worth

mentioning is that although samples that are poled at 75℃ generate the best response to the applied load, according to the hysteresis plots depicted in Figure 17, samples that are poled at higher temperature have higher polarizations, even after compensating for the resistive response (as discussed in Section 3.2.1). A justification for this observation could be that, based on the DOE interaction plots, samples are more sensitive to the changes of temperature at high level of poling duration. For obtaining the hysteresis plots, a frequency of 0.2 *Hz* is used that results in a polarization period of 2.5 seconds for the positive portion of the triangle signal. The DoE results show that a longer polarization time is required for the polarization to be developed at lower temperatures.

4.5 Control Phase

In this phase, a failure mode and effects analysis (FMEA) was performed in order to identify the potential failure modes of the proposed composite structure and suggested methods to detect them. It is worth mentioning that the proposed composite structure is currently at the research and development level. At this point, coupons of composite structure samples are being tested using a set of specific methods. However, in a factory setting, and at volume production levels, some of the current methods are not possible to perform or are very time-consuming. For instance, a tensile test is performed to check the degree of the polarization. However, this method is not applicable for an airplane part that is made of this smart composite material. In order to address this issue, the FMEA is performed at both the research and production manufacturing settings. The FMEA is shown in Table 5.

As shown in Table 5, there are two potential failure modes for the proposed composite structure. The first failure mode is when a short-circuit occurs in the composite structure. The short-circuit failure mode is either due to the imperfections of the composite structure during the fabrication process (such as air bubbles or touching carbon fiber layers), or it is due to the dielectric breakdown during the polarization process. The second potential failure mode is insufficient degree of polarization. As mentioned earlier, the detection methods used for these failures at the research level are not applicable at the industry level. Consequently, suggested methods for failure detection at both research and factory settings are summarized in Table 5.

Table 5.
Failure Modes and Effects Analysis

Item	**Failure Mode**		**Failure Cause**	**Failure Effect**	**Suggested Detection Method**	
					at research level	***at factory setting***
Composite structure	Short-circuit	Before poling	Imperfections (air bubbles or touching carbon fiber layers) during sample fabrication	Corrupted composite, cannot be polarized	Using a multimeter to examine whether a conductive path exists in the composite sample or not.	Check the polarization current, which should be lower than the pre-defined peak current; Check the resistance, which should be higher than the pre-defined minimum resistance
		During poling	Dielectric break down	Corrupted composite, cannot be used for sensing purposes	The current developed in the sample during polarization	
	Insufficient degree of polarization		Incomplete transition to beta phase and insufficient remnant polarization	Weak sensitivity to the applied loads, will not be functional for damage detection	The response of the sample in tensile/compression test and calculating the piezoelectric coefficients	Check the polarization current and compare to pre-defined values at a fully-polarized state ; sample test response of part to applied loads

CHAPTER 5

CHARACTERIZATION RESULTS AND DISCUSSION

5.1 Mechanical Characterization

5.1.1 Young's modulus of composite structure

Figure 22 illustrates the stress-strain plot of the composite sample obtained from the tensile test.

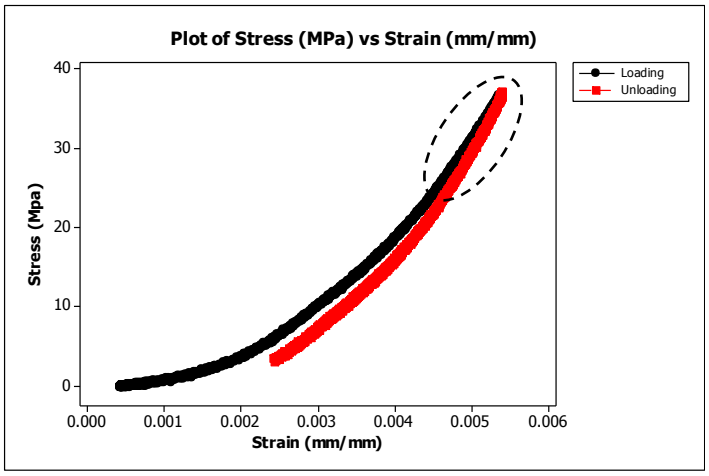

Figure 22. Stress-Strain plot for one of the composite structure's samples

As it can be seen in Figure 22, the strain-stress plot is not linear at the beginning of loading. This is because the composite samples were not perfectly flat due to the applied heat in the polarization process. In order to make sure that there is no bending occurring in the samples, the extensometer was placed at both sides of the sample and the

results confirmed the absence of bending. For calculating the Young's modulus, the last section of the strain-stress plot (as shown in Figure 22) was taken into consideration. For the credibility of the results, two different samples were tested. The Young's modulus for each sample was calculated by averaging the slopes of loading and unloading plots for the two sides of each sample. The final Young's modulus was calculated by averaging the Young's modulus of the two tested samples, which resulted in a modulus of ***E=16.428 Gpa*** for the composite structure. Table 6 summarizes the obtained results.

Table 6.
Results of Young's modulus for the proposed composite structure

			***E* (Gpa)**
Sample 1	Side 1	Loading	16.540
		Unloading	19.609
		Average	18.075
	Side 2	Loading	13.724
		Unloading	17.468
		average	15.596
	Average of both sides (E_1)		16.836
Sample 2	Side 1	Loading	13.197
		Unloading	16.874
		Average	15.036
	Side 2	Loading	14.992
		Unloading	19.012
		average	17.002
	Average of both sides (E_2)		16.019
Composite Structure	avg (E_1 , E_2)		16.428

5.1.2 Young's moduli of carbon fiber and Kevlar materials

Figure 23 and Figure 24 show the stress-strain plots of carbon fiber and Kevlar individual samples, respectively.

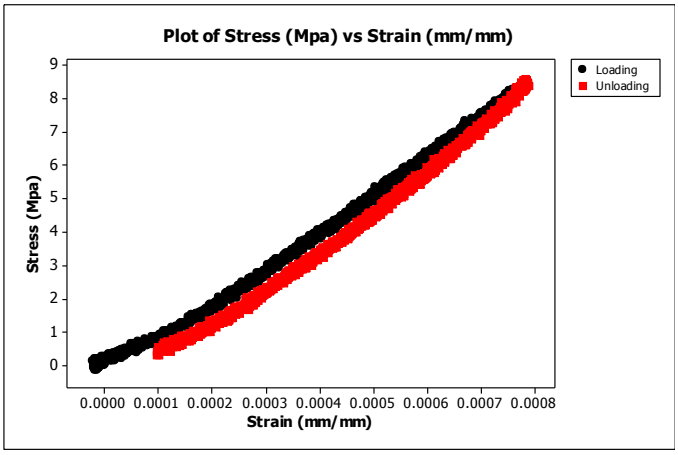

Figure 23. Stress-strain plot for a carbon fiber/PVDF composite

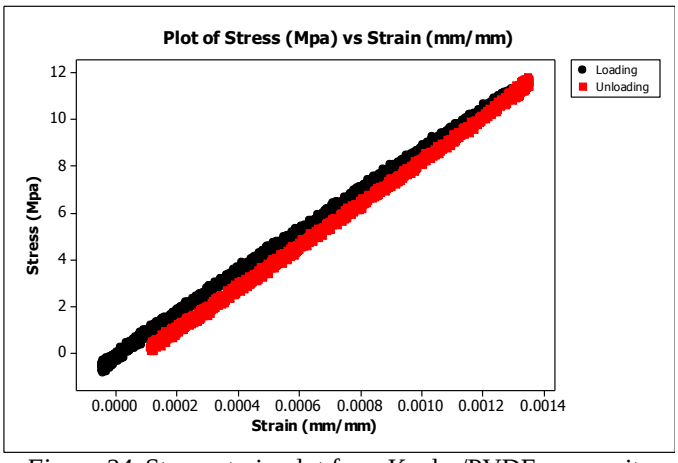

Figure 24. Stress-strain plot for a Kevlar/PVDF composite

For the integrity of results, the last sections of the stress-strain plots were taken into consideration for calculating the Young's modulus. Two different samples were tested for each of the fiber materials. For each tested sample, the Young's modulus was found by averaging the slope of the loading and unloading plots. The Young's modulus of each fiber reinforced composite was calculated by averaging the modulus of their two tested samples. Table 7 summarizes the Young moduli and the volume fractions of fiber material (v_f) and matrix material (v_m) in the tested structures.

Table 7.
Results of Young moduli for Carbon fiber/PVDF and Kevlar/PVDF samples

			Carbon Fiber/PVDF	**Kevlar/PVDF**
ν_f			0.360	0.173
ν_m			0.640	0.827
E	*Sample 1*	*loading*	11.717 Gpa	8.538 Gpa
		unloading	16.352 Gpa	10.155 Gpa
		average (E_1)	14.035 Gpa	9.347 Gpa
	Sample 2	*loading*	10.564 Gpa	5.724 Gpa
		unloading	13.297 Gpa	9.653 Gpa
		average (E_2)	11.931 Gpa	7.688 Gpa
	Composite	*avg(E_1,E_2)*	12.983 Gpa	8.518 Gpa

The results show that the Young's modulus of the Kevlar composite is 65.6% of the modulus of carbon fiber composite. This ratio would be used in Section 5.2.2 for finding the amount of applied force on the middle layer of the composite structure and calculating the d_{31} coefficient.

5.2 Piezoelectric Characterization

5.2.2 d_{31} Coefficient

Figure 25 shows the plot of the force applied to the samples and the charge developed in them during the tensile test.

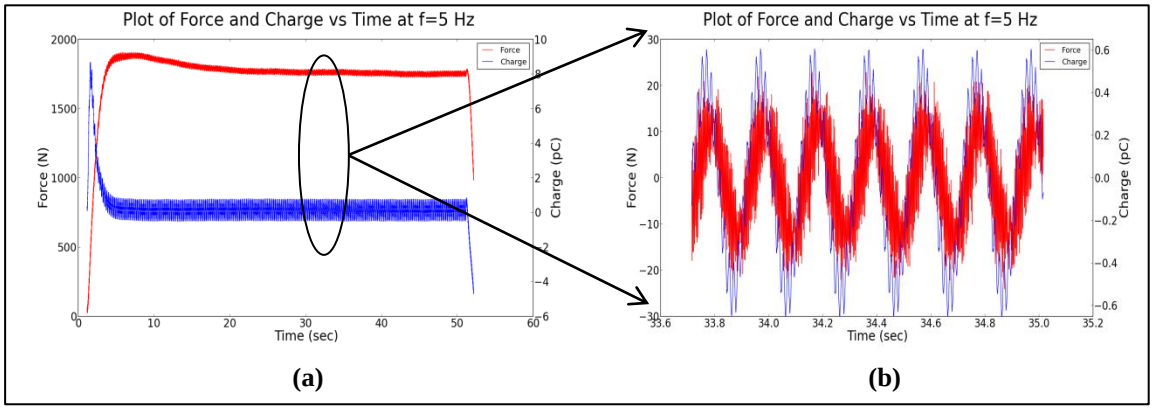

Figure 25. Plots of force and charge vs. time in tensile test (a) complete plot (b) zoomed and plot with DC value removed

According to Figure 25, the amplitude of the applied tensile force was 15.863 *N* and the amplitude of the charge developed in the samples was 0.484 *pC*.

As discussed in Section 3.3.2, in order to find the effective d_{31} coefficient, the amount of applied force between the two carbon fiber layers should be known. Using the formulation discussed in Section 3.3.2, the force applied on the middle layer was found to be 5.587 *N* and the stress on this layer was 0.452 *Mpa*. Finally, knowing the stress on the middle layer and the charge developed on the sample, the $(d_{31})_{eff}$ was calculated as $(d_{31})_{eff} = 1.612\ \mathrm{e}^{-4}\ \frac{pC/m^2}{N/m^2}$. The summary of the procedure for calculating $(d_{31})_{eff}$ is shown in Table A1 in Appendix A.

The obtained value for $(d_{31})_{eff}$ was lower than expected. Three possible reasons for this result have been investigated. First, due to the lower tensile modulus of PVDF compared to Kevlar and Carbon fiber, only a small fraction of total force (~6%) is being transmitted to the PVDF layers in the middle. Because of this small amount of force, the stress developed in the PVDF is low. Second, it is possible that the PVDF layers have not been fully polarized. In order to examine this point, and to determine the degree of

polarization of the PVDF layers, the effective d_{33} coefficient was found in the next section. Using the existing analytical formulation for the effective d_{33} for piezoelectric composite materials, the d_{33} coefficient of PVDF layers can be found. Comparing this value with the existing d_{33} values of PVDF in literature, the degree of polarization of PVDF layers in the composite structure can be investigated. Finally, the electrical impact of the Kevlar dielectric layer could contribute to the low effective d_{31} coefficient.

5.2.3 d_{33} Coefficient

Figure 26 shows the plot of the force applied to the samples and the charge developed in them due to the applied force in the compression test.

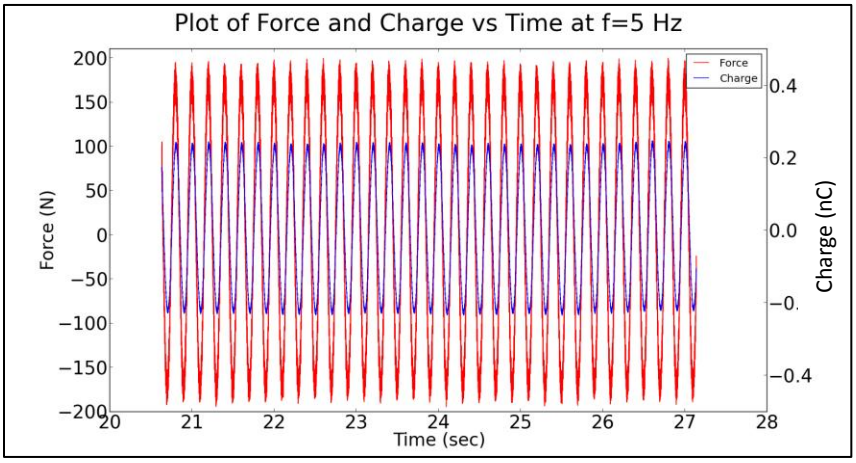

Figure 26. Plots of force and charge vs. time in compression test

As it can be seen in Figure 26, the amplitude of the applied compressive force was 176.28 *N* and the amplitude of the charge developed in the samples was 0.235 *nC*.

As mentioned in Section 3.3.2, in the compression test, the amount of the force applied to the middle layer between the carbon fibers is equal to the total force (176.28 *N*). Consequently, the amount of applied stress on the middle layer is 0.043 *Mpa*.

Knowing the stress on the middle layer and the charge developed on the sample, the effective d_{33} coefficient was found to be $(d_{33})_{eff} = 1.289\ \frac{pC/m^2}{N/m^2}$.

In the next step, the $(d_{33})_{eff}$ was substituted into (10) and the equation was solved for $(d_{33})_{PVDF}$, which yields $(d_{33})_{PVDF}$=3.247 $\frac{pC/m^2}{N/m^2}$. The summary of the procedures for finding $(d_{33})_{eff}$ and $(d_{33})_{PVDF}$ is shown in Table A2 in Appendix A.

Finally, the achieved d_{33} coefficients were compared to the values in the literature as shown in Table 8.

Table 8.
Comparison of the obtained values for d_{33} coefficients with values in literature

		$\boldsymbol{d_{33}}$ $(\frac{pC}{N})$	**Reference**
Bulk PVDF	Experimental	3.247	-
	Theoretical	13-28	(Ramadan et al., 2014)
PVDF in other forms	Proposed composite structure (Carbon Fiber-Kevlar/PVDF)	1.289	-
	PZT/PVDF-HFP 50/50 vol %	25	(Malmonge, Malmonge, & Sakamoto, 2003)
	PVDF-HFP 90:10	3	(Malmonge et al., 2003)
	PVDF-TrFE	22.1	(Zeng, Kwok, Chan, & Choy, 2002)
	30%$BaTiO3_{(whiskers)}$/PVDF(normal) with poling field 3 KV/mm	13.7	(Chen et al., 2004)
	30%$BaTiO3_{(powder)}$/PVDF with poling field 3 KV/mm	4.4	(Chen et al., 2004)

The obtained result for the piezoelectric coefficients suggests that some degree of polarization has been achieved and it confirms the sensing capability of the proposed composite structure. However, the comparison of the experimental values of the piezoelectric constants with values in literature shows that there is still potential for the

enhancement of the degree of polarization to achieve improved sensitivity. This will be a part of future effort for this project, which is discussed in Section 7.2.

CHAPTER 6

FUTURE MARKET POTENTIAL

In the previous chapters, the concept and the development of the proposed carbon fiber reinforced composite were discussed. In this chapter, the proposed composite structure will be examined from the market perspective and its future market potential and competency will be studied.

First, a SWOT analysis was performed in order to assess the strengths, weaknesses, opportunities, and threats contributing to this product, which helps in developing effective strategies for ensuring the success of this product in the future. Figure 27 summarizes the results of the SWOT analysis.

Based on the SWOT analysis, a few recommendations have been made to help the future success of the proposed product. From the mentioned weaknesses, the degree of polarization is the most critical one, because it also contributes to the threats of other competitors and reluctancy of implementation. Not addressing this weakness would result in the intensification of the threats, and consequently, a major failure for the product. As a result, this weakness should be eliminated in order to alleviate the threats and increase the competency of the product. Moreover, the strengths that contribute to the mentioned opportunities, such as the self-sensing potential for SHM and the lower processing temperature, should be given special consideration. Because these are the competent

capabilities that can help the product stand out in the future market. Focusing on these strengths during the commercialization and marketing process can help in the future success of this composite structure.

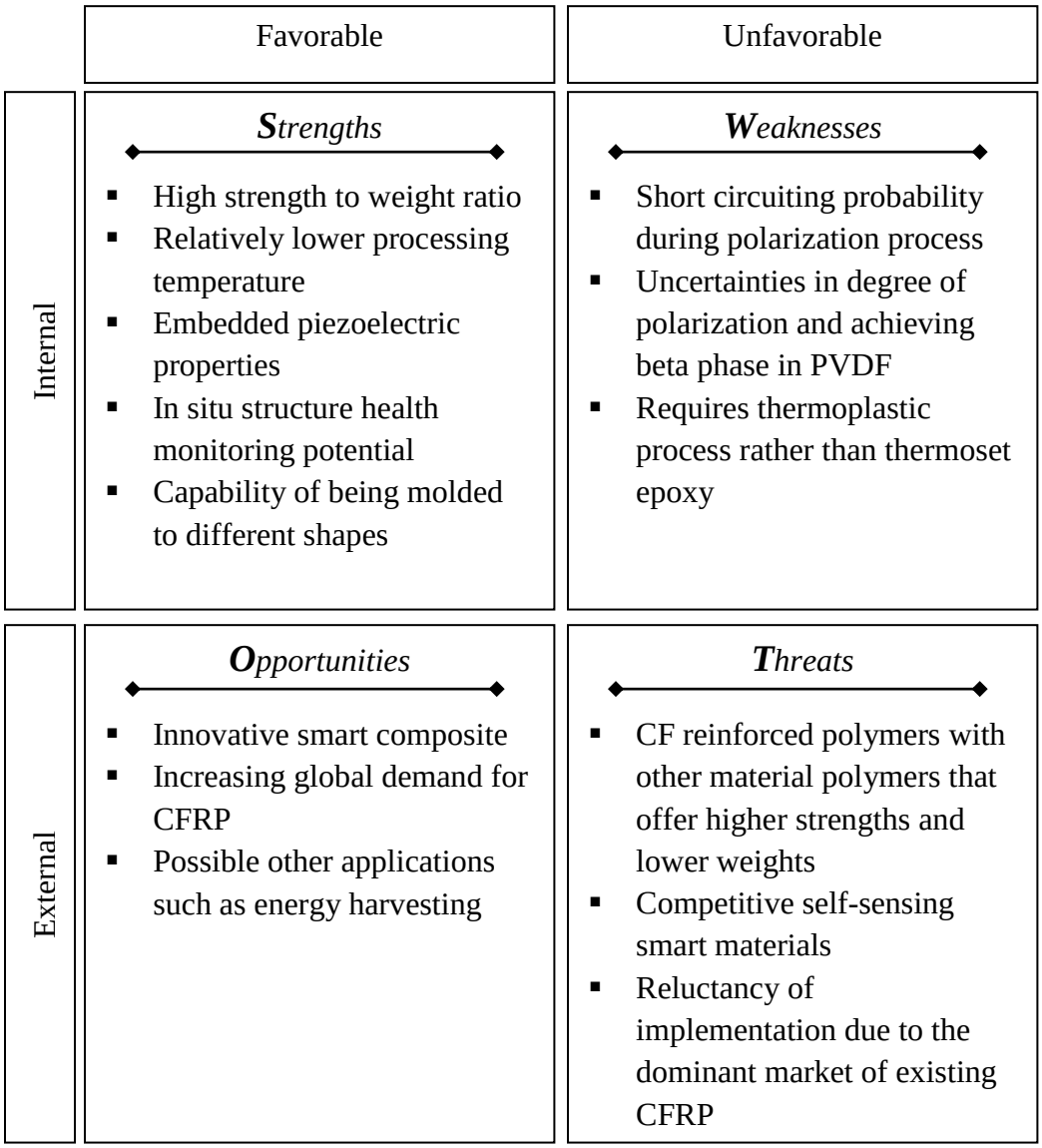

Figure 27. SWOT analysis for the proposed composite structure

As discussed earlier, carbon fiber reinforced composites are being widely used in different industries. According to a survey by *Carbon Composites e.V.* (CCeV, which is an organization dedicated to research and business in the high-performance fiber reinforced composite sector, based in Germany, Austria and Switzerland), and as discussed by Holmes (2013), 95% of the carbon fiber used in fabricating carbon fiber-reinforced composites is for developing carbon fiber reinforced plastics (CFRP) (Holmes, 2013). Moreover, based on the data provided by CCeV (Holmes, 2013), in 2012, the global demand for CFRP has an increasing trend in the near future (see Figure 28).

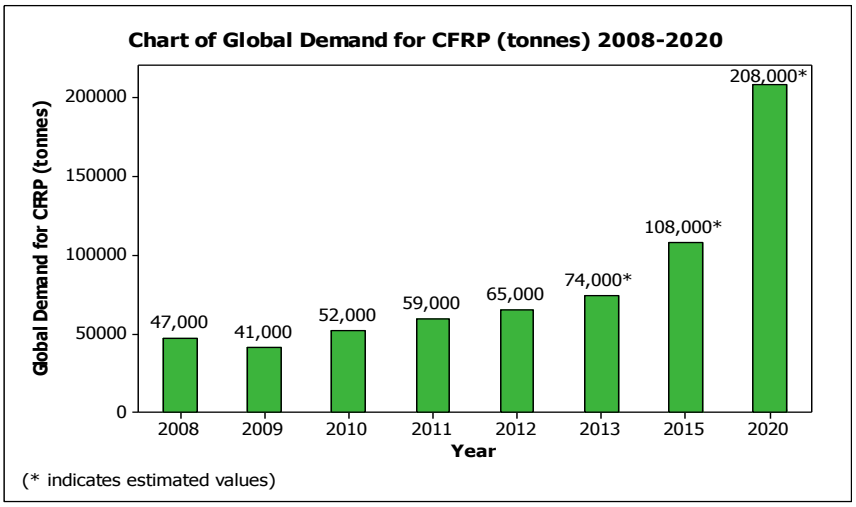

Figure 28. Global demand for carbon fiber-reinforced plastics for years 2008-2020 [Data from (Holmes, 2013)]

Based on the fact that the proposed composite structure in this study can be classified as a CFRP composite and considering the increasing global demand for this type of composite, it can be inferred that there would be potential market demand for the proposed composite structure. The next question to consider is which industries or applications are potential target customers of this proposed composite. In order to find the answer to this question, the data of global carbon fiber consumption by application

presented by CCeV and discussed by Holmes (2013) is investigated (Holmes, 2013). Figure 29 represents the chart of global carbon fiber consumption in different applications in year 2012 (Holmes, 2013).

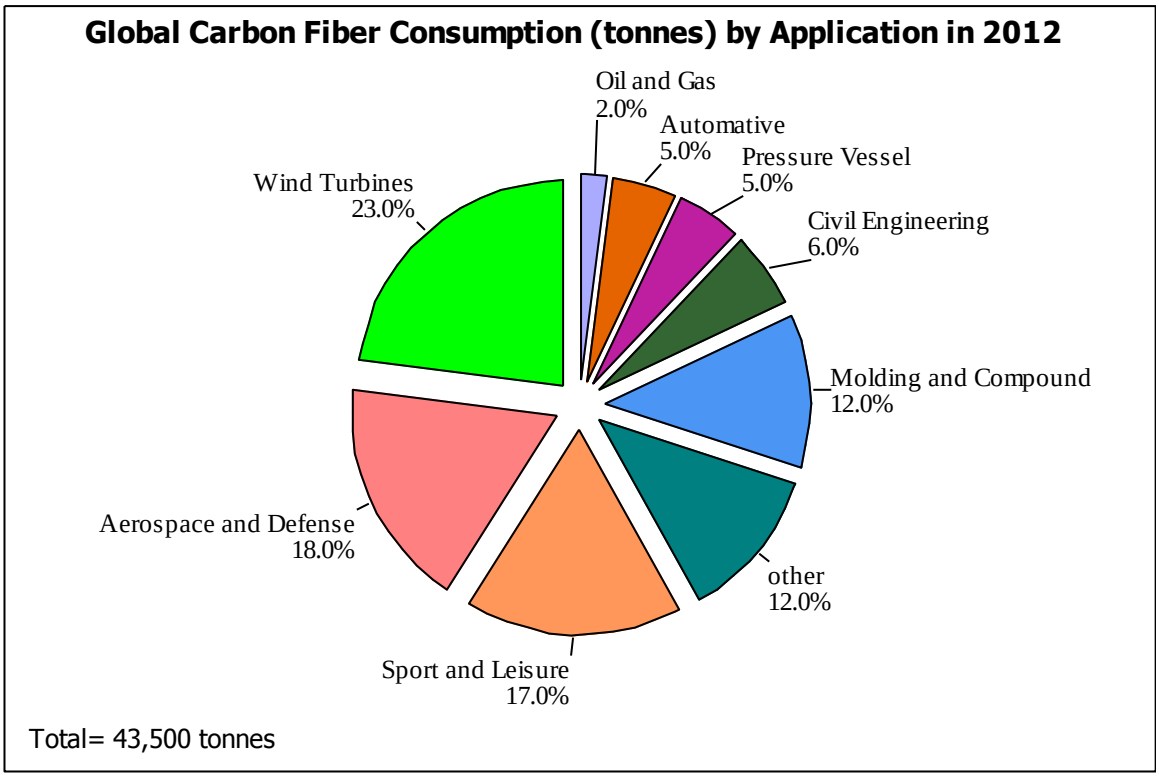

Figure 29. Global carbon fiber consumption by application in year 2012 [Data from (Holmes, 2013)]

As it can be seen in Figure 29, wind turbines, and aerospace and defense have the highest carbon fiber consumption, respectively. In addition, in both of these industries, structural health monitoring is necessary for assuring the safety, reliability, and efficient performance of the structure. Based on the SWOT analysis, the high strength to weight ratio of the proposed composite structure can contribute to the requirements in these two industries. Besides, as discussed in the SWOT analysis, the in-situ health monitoring capability of the proposed smart composite can facilitate the structural health monitoring process in these two application areas. Consequently, these two market segments are the

potential target customers of the proposed composite structure. The carbon fiber-reinforced composite developed in this study have great potential for use in these two market segments, as well as potentially satisfying the need for structural health monitoring in other applications yet to be identified.

In order to have a better understanding of the future market for the proposed composite structure and develop effective strategies for its success, different marketing analysis tools were implemented. First, Ansoff's matrix was used to determine the type of market and product that the proposed composite structure fits into. Ansoff's matrix is a strategic tool that helps businesses to choose the best option for their growth. Ansoff Matrix proposes four different types of marketing strategies based on the type of the product (new or existing) and the type of the market (new or existing). These four strategies are classified as: market penetration, product development, market development, and diversification (Ansoff, 1957) (see Figure 30).

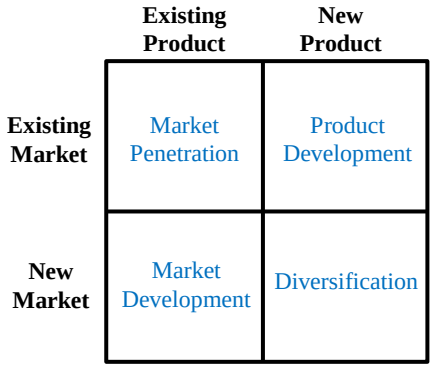

Figure 30. Ansoff Matrix

The proposed smart composite structure will fit into the "product development" quadrant of Ansoff Matrix. This is because the market for CFRP and smart structures exists, while this study proposes a new product with new and improved features.

Furthermore, the technology S-curves for developments in composite industry was investigated to identify the current situation of the proposed composite structure. Figure 31 illustrates the individual S-curves proposed for developments in the composite materials (Rojko, Lesjak, & Vehovar, 2011). This plot was developed based on a classification for different generations of composites suggested by Palucka and Bensaude-Vincent (Palucka & Bensaude-Vincent, 2002).

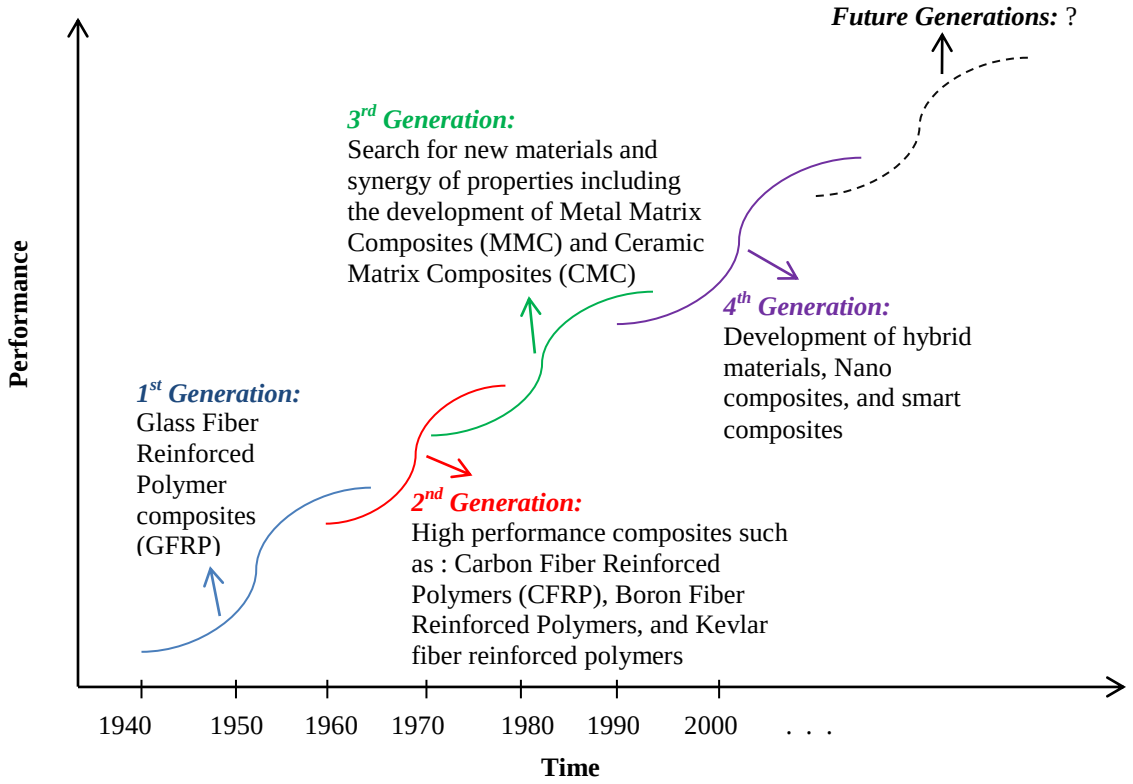

Figure 31. Development of composite materials through individual S-curves [Modified from(Rojko, Lesjak, & Vehovar, 2011)]

Each individual S-curve represents the lifecycle required for development in each of the composites' generations from its inception to its maturity and saturation

(Christensen, 1992). This lifecycle consists of four main stages: Invention, Improvement and Growth, Maturity, and Aging (Bowden, 2004) (see Figure 32).

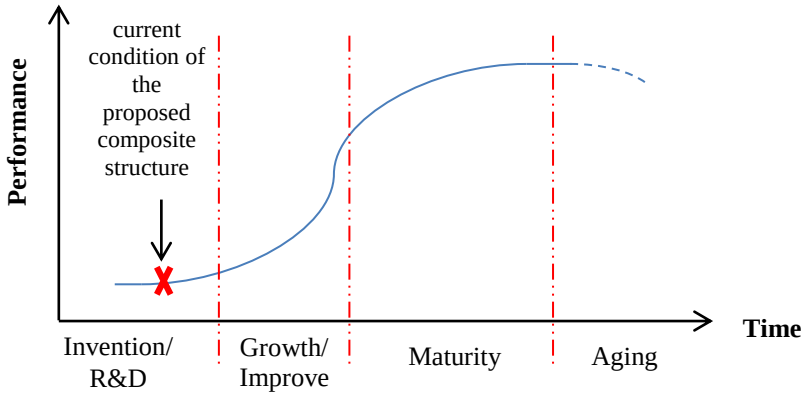

Figure 32. Technology S-curve [Modified from (Bowden, 2004)]

As indicated in Figure 31, the proposed composite structure is currently in the embryonic stage. Implementing effective strategies based on the discussion in this chapter will help in the successful transition of this proposed technology to the next stages and, consequently, will help in its success in the future market.

CHAPTER 7

CONCLUSIONS AND FUTURE WORK

7.1 Concluding Remarks

This study introduced the concept of a new carbon fiber-reinforced polymer composite and the preliminary results of its development. The main difference of this proposed composite with other CFRP composites is that the common polymers typically used for the matrix material has been replaced with the piezoelectric polymer PVDF. The piezoelectricity of PVDF as the matrix material, along with the electrical conductivity of carbon fibers as the reinforcement material, enable this composite to have integrated force sensing capabilities that can be used for in situ structural health monitoring of CFRP structures.

Throughout this study, the fabrication process of the composite samples used in the experiments was discussed. In order for the prepared composite samples to generate response to applied loads in tensile and compression tests, they need to be polarized to align the dipoles in the crystalline phase of the PVDF material. Using the DMAIC approach, the main factors affecting the polarization process were identified as voltage, temperature, and duration of poling. By performing a full factorial DOE, the impact of these factors and their optimal conditions for polarization process were investigated. The results showed that high levels of voltage and duration of polarization have a positive

impact on the charge generated by samples when exposed to an applied load. However, the effect of temperature was non-linear. Given the temperatures that were tested in this study, poling at 75 ℃ showed the highest response.

Next, the proposed composite structure was characterized from both mechanical and piezoelectric perspectives. For the mechanical characterization, the Young's modulus of the composite was investigated as a measure of its stiffness. The results showed an average Young's modulus of 16.428 *Gpa* for the composite. For the purpose of piezoelectric characterization, the piezoelectric coefficients d_{31} and d_{33} were studied in tensile and compression tests, respectively. The experiments led to effective piezoelectric coefficients of $(d_{31})_{eff} = 1.612\ \mathrm{e}^{-4}\ \frac{pC/m^2}{N/m^2}$ and $(d_{33})_{eff} = 1.289\ \frac{pC/m^2}{N/m^2}$ for the proposed composite structure. These results confirmed the potential capability of this composite structure to act as an integrated sensor. In addition, the comparison of these results with literature values suggests that there is capacity for further enhancements in the degree of polarization.

Finally, the future market of this composite structure was studied. It was observed that the global demand for CFRP has a growing trend in the next years. Moreover, wind turbines and aerospace were identified as the potential target customers of this composite based on their carbon fiber composites consumption and the functional contribution of the proposed composite to these applications. In addition, different marketing analysis tools including the Ansoff's Matrix, technology S-curve, and the SWOT analysis were implemented to identify the current condition of this composite as a product in the market and develop effective strategies to ensure its success and growth in the future.

7.2 Future Work

Based on the results achieved for the piezoelectric coefficients, the future work for this project involves improving the degree of polarization and consequently, the piezoelectric coefficients. For this purpose, two methods have been suggested. In the first method, the samples will be cured under an applied electric field during the sample fabrication process. In the second proposed method, the samples will be cooled down under the applied electric field during the polarization process.

In addition, the practical application of this composite structure as a sensor for failure detection and in situ structural health monitoring will be investigated. For this purpose, a meshed structure was proposed as shown in Figure 33. In order to evaluate the potential of the composite for failure detection, a notch will be applied on one of the elements (see Figure 33(a)).

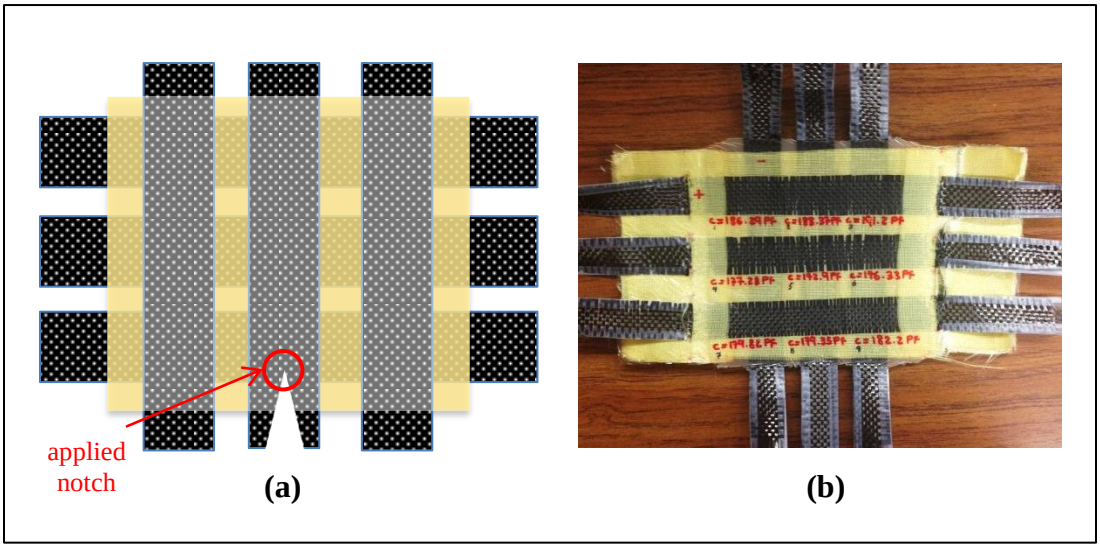

Figure 33. Proposed meshed composite structure for evaluating damage detection, (a) schematic of the structure and the applied notch, (b) prepared meshed composite structure

REFERENCES

Aboelmaged, M. G. (2010). Six Sigma quality: a structured review and implications for future research. *International Journal of Quality & Reliability Management*, *27*(3), 268–317.

Abot, J. L., Song, Y., Vatsavaya, M. S., Medikonda, S., Kier, Z., Jayasinghe, C., … Schulz, M. J. (2010). Delamination detection with carbon nanotube thread in self-sensing composite materials. *Composites Science and Technology*, *70*(7), 1113–1119.

Akhras, G. (2000). Smart materials and smart systems for the future. *Canadian Military Journal*, *1*(3), 25–31.

Ansoff, H. I. (1957). Strategies for diversification. *Harvard Business Review*, *35*(5), 113–124.

Antony, J. (2014). Design of Experiments and its Role Within Six Sigma. In *Design of Experiments for Engineers and Scientists* (pp. 201–208). Elsevier.

Bhalla, A. S., Oururaja, T. R., Haertling, G. H., Smyth, D. M., Vest, R. W., Tancrell, R. H., … others. (1986). Standard Definitions of Primary Ferroelectric Terms. *IEEE Transactions on Ultrasonics, Ferroelectrics, and Frequency Control*, *410*, 765–4290.

Bloomfield, P. E. (1988). Production of Ferroelectric Oriented Pvdf Films. *Journal of Plastic Film and Sheeting*, *4*(2), 123–129.

Bowden, M. J. (2004). Moore's Law and the Technology S-Curve. *Current Issues in Technology Management, Stevens Alliance for Technology Management*, *8*(1).

Cao, W., Cudney, H. H., & Waser, R. (1999). Smart materials and structures. *Proceedings of the National Academy of Sciences*, *96*(15), 8330–8331.

Chand, S. (2000). Review Carbon fibers for composites, *35*(6), 1303–1313.

Chen, L. F., Hong, Y. P., Chen, X. J., Wu, Q. L., Huang, Q. J., & Luo, X. T. (2004). Preparation and properties of polymer matrix piezoelectric composites containing aligned BaTiO3 whiskers. *Journal of Materials Science*, *39*(9), 2997–3001.

Christensen, C. M. (1992). Exploring the Limits of the Technology S-Curve. Part I: Component Technologies. *Production and Operations Management*, *1*(4), 334–357.

Chung, D. D. L. (1994). *Carbon Fiber Composites*. Elsevier.

Costa, C. M., Sencadas, V., Mano, J. F., & Lanceros-Méndez, S. (2006). Effect of poling on the mechanical properties of β-poly (vinylidene fluoride). In *Materials science forum* (Vol. 514, pp. 951–955). Trans Tech Publ.

Dargaville, T. R., Celina, M. C., Elliott, J. M., Chaplya, P. M., Jones, G. D., Mowery, D. M., … Martin, J. W. (2005). *Characterization, performance and optimization of PVDF as a piezoelectric film for advanced space mirror concepts*. Sandia National Laboratories.

Davis, G. T., McKinney, J. E., Broadhurst, M. G., & Roth, S. C. (1978). Electric-field-induced phase changes in poly(vinylidene fluoride). *Journal of Applied Physics, 49*(10), 4998.

Deteresa, S. J., Allen, S. R., Farris, R. J., & Porter, R. S. (1984). Compressive and torsional behaviour of Kevlar 49 fibre. *Journal of Materials Science*, *19*(1), 57–72.

Dickens, B., Balizer, E., DeReggi, A. S., & Roth, S. C. (1992). Hysteresis measurements of remanent polarization and coercive field in polymers. *Journal of Applied Physics*, *72*(9), 4258.

Etzold, K. F. (2000). Ferroelectric and Piezoelectric Materials. In R. C. Dorf (Ed.), *The Electrical Engineering Handbook*. Boca Raton: CRC Press.

Fraden, J. (2010). *Handbook of Modern Sensors: Physics, Design, and Applications* (4th ed.). Springer.

George, M. L. (2002). *Lean Six Sigma: Combining Six Sigma Quality with Lean Production Speed*. McGraw-Hill.

Guemes, J. A., & Menendez, J. M. (2002). Response of Bragg grating fiber-optic sensors when embedded in composite laminates. *Composites Science and Technology*, *62*(7), 959–966.

Harmon, P. (Ed.). (2014). Incremental Improvement with Lean and Six Sigma. In *Business Process Change (Third Edition)* (pp. 293–325). Boston: Morgan Kaufmann.

Harper, C. A. (Ed.). (1999). *Modern Plastics Handbook*. McGraw-Hill.

Holmes, M. (2013). Carbon fibre reinforced plastics market continues growth path. *Reinforced Plastics*, *57*(6), 24–29.

Hsu, C. C., & Geil, P. H. (1984). Morphology-structure-property relationships in ultraquenched poly(vinylidene fluoride). *Journal of Applied Physics*, *56*(9), 2404.

Hsu, S. L., Lu, F. J., Waldman, D. A., & Muthukumar, M. (1985). Analysis of the crystalline phase transformation of poly(vinylidene fluoride). *Macromolecules, 18*(12), 2583–2587.

Huang, X. (2009). Fabrication and Properties of Carbon Fibers. *Materials*, *2*(4), 2369–2403.

Jones, R. M. (1998). *Mechanics of Composite Materials* (2nd ed.). CRC Press.

Kepler, R. G., & Anderson, R. A. (1992). Ferroelectric polymers. *Advances in Physics, 41*(1), 1–57.

Kessler, S. S., Spearing, S. M., & Soutis, C. (2002). Damage detection in composite materials using Lamb wave methods. *Smart Materials and Structures*, *11*(2), 269.

Kollár, L. P., & Springer, G. S. (2003). *Mechanics of Composite Structures*. Cambridge University Press.

Kuang, Ksc., Kenny, R., Whelan, M. P., Cantwell, W. J., & Chalker, P. R. (2001). Embedded fibre Bragg grating sensors in advanced composite materials. *Composites Science and Technology*, *61*(10), 1379–1387.

Leng, J., & Asundi, A. (2003). Structural health monitoring of smart composite materials by using EFPI and FBG sensors. *Sensors and Actuators A: Physical*, *103*(3), 330–340.

Li, M.-H. C., Al-Refaie, A., & Cheng-Yu Yang. (2008). DMAIC Approach to Improve the Capability of SMT Solder Printing Process. *IEEE Transactions on Electronics Packaging Manufacturing, 31*(2), 126–133.

Lissenden, C. J., & Rose, J. L. (2008). Structural Health Monitoring of Composite Laminates Through Ultrasonic Guided Wave Beam Forming. In *NATO Applied Vehicle Technology Symposium on Military Platform Ensured Availability Proceedings*.

Lovinger, A. J. (1982). Poly(vinylidene fluoride). In D. C. Basset (Ed.), *Developments in Crystalline Polymers* (pp. 195–273). London: Applied Science Publishers.

Loyola, B. R., Briggs, T. M., Arronche, L., Loh, K. J., La Saponara, V., O'Bryan, G., & Skinner, J. L. (2013). Detection of spatially distributed damage in fiber-reinforced polymer composites. *Structural Health Monitoring*, *12*(3), 225–239.

Malmonge, L. F., Malmonge, J. A., & Sakamoto, W. K. (2003). Study of pyroelectric activity of PZT/PVDF-HFP composite. *Materials Research*, *6*(4), 469–473.

Mathews, P. G. (2005). *Design of Experiments with MINITAB*. American Society for Quality (ASQ).

Matthews, F. L., & Rawlings, R. D. (1999). *Composite Materials: Engineering and Science*. Elsevier.

Mohammadi, B., Yousefi, A. A., & Bellah, S. M. (2007). Effect of tensile strain rate and elongation on crystalline structure and piezoelectric properties of PVDF thin films. *Polymer Testing*, *26*(1), 42–50.

Moheimani, S. R., & Fleming, A. J. (2006). *Piezoelectric transducers for vibration control and damping*. Springer.

Montgomery, D. C. (2008). *Design and Analysis of Experiments*. John Wiley & Sons.

Murukeshan, V. M., Chan, P. Y., Ong, L. S., & Seah, L. K. (2000). Cure monitoring of smart composites using fiber Bragg grating based embedded sensors. *Sensors and Actuators A: Physical*, *79*(2), 153–161.

Neelakanta, P. S. (1995). Piezoelectric Composite Materials. In *Handbook of Electromagnetic Materials: Monolithic and Composite Versions and Their Applications* (1st ed., pp. 293–305). CRC Press.

Ong, W. H., & Chiu, W. K. (2013). Enhancement of Lamb wave-based in situ structural health monitoring through guided local geometry changes. *Structural Health Monitoring*, *12*(4), 339–358.

Palucka, T., & Bensaude-Vincent, B. (2002). *Composites Overview*. *Dibner Institute for the History of Science and Technology at MIT*.

Professional Plastics. (n.d.). PVDF Film – Material Data Sheet. Retrieved June 27, 2014 from www.professionalplastics.com/professionalplastics/content/PVDFFilmDataSheet.doc

Ramadan, K. S., Sameoto, D., & Evoy, S. (2014). A review of piezoelectric polymers as functional materials for electromechanical transducers. *Smart Materials and Structures*, *23*(3), 033001.

Rojko, K., Lesjak, D., & Vehovar, V. (2011). Information communication technology spending in (2008-) economic crisis. *Industrial Management & Data Systems*, *111*(3), 391–409.

Sajkiewicz, P., Wasiak, A., & Goclowski, Z. (1999). Phase transitions during stretching of poly(vinylidene fluoride). *European Polymer Journal*, *35*, 423–429.

Saulnier, G. J., Blue, R. S., Newell, J. C., Isaacson, D., & Edic, P. M. (2001). Electrical impedance tomography. *Signal Processing Magazine, IEEE, 18*(6), 31–43.

Sirohi, J., & Chopra, I. (2000). Fundamental Understanding of Piezoelectric Strain Sensors. *Journal of Intelligent Material Systems and Structures, 11*(4), 246–257.

Sokovic, M., Pavletic, D., & Pipan, K. K. (2010). Quality improvement methodologies–PDCA cycle, RADAR matrix, DMAIC and DFSS. *Journal of Achievements in Materials and Manufacturing Engineering, 43*(1), 476–483.

Song, D., Yang, D., & Feng, Z. (1990). Formation of β-phase microcrystals from the melt of PVF2-PMMA blends induced by quenching. *Journal of Materials Science, 25*(1), 57–64.

Staszewski, W. J., Boller, C., & Tomlinson, G. R. (2004). Aircraft Structural Health and Usage Monitoring. In *Health monitoring of aerospace structures smart sensor technologies and signal processing* (pp. 29–71). Chichester, West Sussex, England; Hoboken, NJ: J. Wiley.

Stewart, M., Cain, M. G., & Hall, D. A. (1999). *Ferroelectric Hysteresis Measurement & Analysis* (No. NPL Report CMMT(A) 152).

Talbot, D. (2003). *Smart Material*. Institute of Materials, Minerals and Mining.

Tenera, A., & Pinto, L. C. (2014). A Lean Six Sigma (LSS) Project Management Improvement Model. *Procedia - Social and Behavioral Sciences, 119*, 912–920.

Thomas, A., Barton, R., & Chuke-Okafor, C. (2009). Applying lean six sigma in a small engineering company – a model for change. *Journal of Manufacturing Technology Management, 20*(1), 113–129.

Tichý, J., Erhart, J., Kittinger, E., & Prívratská, J. (2010). *Fundamentals of Piezoelectric Sensorics: Mechanical, Dielectric, and Thermodynamical Properties of Piezoelectric Materials*. Springer.

Tong, J. P. C., Tsung, F., & Yen, B. P. C. (2004). A DMAIC approach to printed circuit board quality improvement. *The International Journal of Advanced Manufacturing Technology, 23*(7-8), 523–531.

Wang, H. (2008). A review of six sigma approach: methodology, implementation and future research. In *Wireless Communications, Networking and Mobile Computing, 2008. WiCOM'08. 4th International Conference on* (pp. 1–4). IEEE.

Zeng, R., Kwok, K. W., Chan, H. L. W., & Choy, C. L. (2002). Longitudinal and transverse piezoelectric coefficients of lead zirconate titanate/vinylidene fluoride-

trifluoroethylene composites with different polarization states. *Journal of Applied Physics*, *92*(5), 2674.

APPENDIX A:

PROCEDURES FOR CALCULATING THE EFFECTIVE PIEZOELECTRIC COEFFICIENTS d_{31} AND d_{33}

Table A1. Summary of the procedure for calculating $(d_{31})_{eff}$

Step	Equations	Known Parameters	Solve for: (unknown parameters)	Results
1	1. $k_{tot} = 2k_{CF} + k_{K+PVDF} \rightarrow \frac{E_{tot}A_{tot}}{L_{tot}} = 2\frac{E_{CF}A_{CF}}{L_{CF}} + \frac{E_{K+PVDF}A_{K+PVDF}}{L_{K+PVDF}}$ (where: $A = t \times w$ & $assume\ w_{CF} = w_{K+PVDF} = w_{tot}; L_{CF} = L_{K+PVDF} = L_{tot}$) 2. $E_{K+PVDF} = 0.656\ E_{CF}$	$t_{tot} = 0.682\ mm$	E_{CF}	19.46 Gpa
		$t_{CF} = 0.373\ mm$		
		$t_{K+PVDF} = 0.309\ mm$	E_{K+PVDF}	12.77 Gpa
		$E_{tot} = 16.428\ Gpa$		
2	1. $\delta_{CF} = \delta_{K+PVDF} \rightarrow \frac{F_{CF}L_{CF}}{E_{CF}A_{CF}} = \frac{F_{K+PVDF}L_{K+PVDF}}{E_{K+PVDF}A_{K+PVDF}}$ (where: $A = t \times w$ & $assume\ w_{CF} = w_{K+PVDF} = w_{tot}; L_{CF} = L_{K+PVDF} = L_{tot}$) 2. $F_{tot} = 2F_{CF} + F_{K+PVDF}$	$t_{CF} = 0.373\ mm$	F_{CF}	10.278 N
		$t_{K+PVDF} = 0.309\ mm$		
		$E_{CF} = 19.46$ Gpa		
		$E_{K+PVDF} = 12.77$ Gpa	F_{K+PVDF}	5.587 N
		$F_{tot} = 15.865\ N$		
3	$\sigma_{K+PVDF} = \frac{F_{K+PVDF}}{A_{K+PVDF}}$	$F_{K+PVDF} = 5.587\ N$	σ_{K+PVDF}	0.452 Mpa
		$A_{K+PVDF} = 12.36\ mm^2$		
4	$(d_{31})_{eff} = \frac{Q/A_{CF,electrode}}{\sigma_{K+PVDF}}$	$Q = 0.484\ pC$	$(d_{31})_{eff}$	$1.612e^{-4}$ $\frac{pC/m^2}{N/m^2}$
		$A_{CF,electrode} = 0.0028\ m^2$		
		$\sigma_{K+PVDF} = 0.452\ Mpa$		

Table A2. Summary of the procedures for calculating $(d_{33})_{eff}$ and $(d_{33})_{PVDF}$

Step	Equations	Known Parameters	Solve for: (unknown parameters)	Results
1	$\sigma_{K+PVDF} = \frac{F_{K+PVDF}}{A_{K+PVDF}}$ (where: $F_{K+PVDF} = F_{tot}$)	$F_{K+PVDF} = 176.28\ N$ $A_{K+PVDF} = 4.072e^{-3}\ m^2$	σ_{K+PVDF}	0.043 Mpa
2	$(d_{33})_{eff} = \frac{Q/A_{CF,electrode}}{\sigma_{K+PVDF}}$	$Q = 0.2345\ nC$ $A_{CF,electrode} = 0.0042\ m^2$ $\sigma_{K+PVDF} = 0.043\ Mpa$	$(d_{33})_{eff}$	1.289 $\frac{pC/m^2}{N/m^2}$
3	$(d_{33})_{eff} = \frac{v_{PVDF}(d_{33})_{PVDF}(\varepsilon_{33})_K + v_K(d_{33})_K(\varepsilon_{33})_{PVDF}}{v_{PVDF}(\varepsilon_{33})_K + v_K(\varepsilon_{33})_{PVDF}}$	$(d_{33})_{eff} = 1.289\ \frac{pC/m^2}{N/m^2}$ $v_{PVDF} = 0.605$ $v_K = 0.395$ $(\varepsilon_{33})_{PVDF} = 9.305$ $(\varepsilon_{33})_K = 4$ $(d_{33})_{Kevlar} = 0$	$(d_{33})_{PVDF}$	3.247 $\frac{pC/m^2}{N/m^2}$